



Technical Report:
**Compressor, Expander &
Mechanical Drive System**

Summary

In this paper a method is suggested for optimising reversible scroll compressor/expander design for small scale operation. This was part of a research program to develop a Pumped Thermal Energy Storage System for use in the bottom 50 Human Development Index countries, the majority of which are in Sub-Saharan Africa. The scroll optimisation was based on the modelling of a profile to achieve a required compression ratio from first principles. This was followed by a detailed mechanical design of the linkage between two compressor/ expander units and a motor/ generator. It was concluded that the scroll profiling was successful and could be applied for a variety of different scenarios. The mechanical design proposed was functional though untested. The work done here represents the first iteration of what should certainly be a multistage process for development of a product such as this. Recommended future work includes CFD of the proposed compressor in order that further development on this work can be made.

Sam Riddell-Webster

Table of Contents

INTRODUCTION	4
PUMPED THERMAL ENERGY STORAGE SYSTEM LAYOUT 295 5267	5
SUB ASSEMBLY REQUIREMENTS	6
PRODUCT SCOPING	7
SCALING APPROXIMATIONS	9
SUB-SYSTEM: REVERSIBLE COMPRESSOR/ EXPANDER WITH MECHANICAL DRIVE SYSTEM	12
PRODUCT DESIGN SPECIFICATION	13
SCROLL COMPRESSOR GEOMETRY	14
SCROLL PROFILE	15
INNER SCROLL PROFILE DEFINITION	17
SINGLE ARC TIP PROFILE	17
VOLUME DETERMINATION	19
DESIGN OPTIMISATION OF SCROLL PROFILE	21
INPUT PARAMETERS	21
SOFTWARE FLOW DIAGRAM	22
OPTIMISATION SEQUENCE METHODOLOGY	23
OPTIMISATION OF SCROLL HEIGHT AND OPERATING SPEED	25
SCROLL VOLUME VALIDATION	26
PRODUCT REQUIREMENT SPECIFICATION	27
INITIAL CONCEPT DESIGN	28
MORPHOLOGICAL CHART	28
CONTROLLED CONVERGENCE	29
CONCEPT DESIGN: FULL MECHANICAL LINKAGE SYSTEM - SPRAG CLUTCH	31
DESIGN EMBODIMENT	32
COMPRESSOR/ EXPANDER 1	33
COMPRESSOR/ EXPANDER 2	36
MECHANICAL LINKAGE	37
MOTOR SELECTION	37
CONCLUSION	39
BIBLIOGRAPHY	40
APPENDIX I	42
APPENDIX II	48
APPENDIX III	56

Introduction

Currently 1.2 billion people globally live with limited or no electricity. 60% of these people live in Sub Saharan Africa, a region with huge potential for solar electrical generation. The price of photovoltaic cells is becoming ever more affordable as the technology advances but there are currently no sustainable methods of storing this power. Lithium ion batterie performance reduces drastically over a five-year period and this degradation is increased by high temperature operation.

This series of papers [1–5], present a detailed design plan for optimisation of a Pumped Heat Thermal Energy Storage (PTES) system [6], for use in rural African villages. In this paper, user research was conducted for the target area to aid in a scaling approximation for the product.

A detailed design optimisation was carried out for the use of reversible scroll compressor/ expansion units from first principles based on the work of Blunier et al [7] and other research on the same topic ,in order to develop a working model that could generate scroll profiles suitable for use in the PTES system. This was then followed by a detailed mechanical design of the compressor/ expanders and mechanical linkage with the rest of the system.

Pumped Thermal Energy Storage System Layout

The system design is a small scale Pumped Thermal Energy Storage System (PTES) [6]. The basic concept is that the system functions as an electricity storage system for people in rural environments with no access to grid electricity. Early research showed that around 65% [8] of people without electricity live in Sub-Saharan Africa (SSA) and so this product is primarily targeted at this user demographic [9].

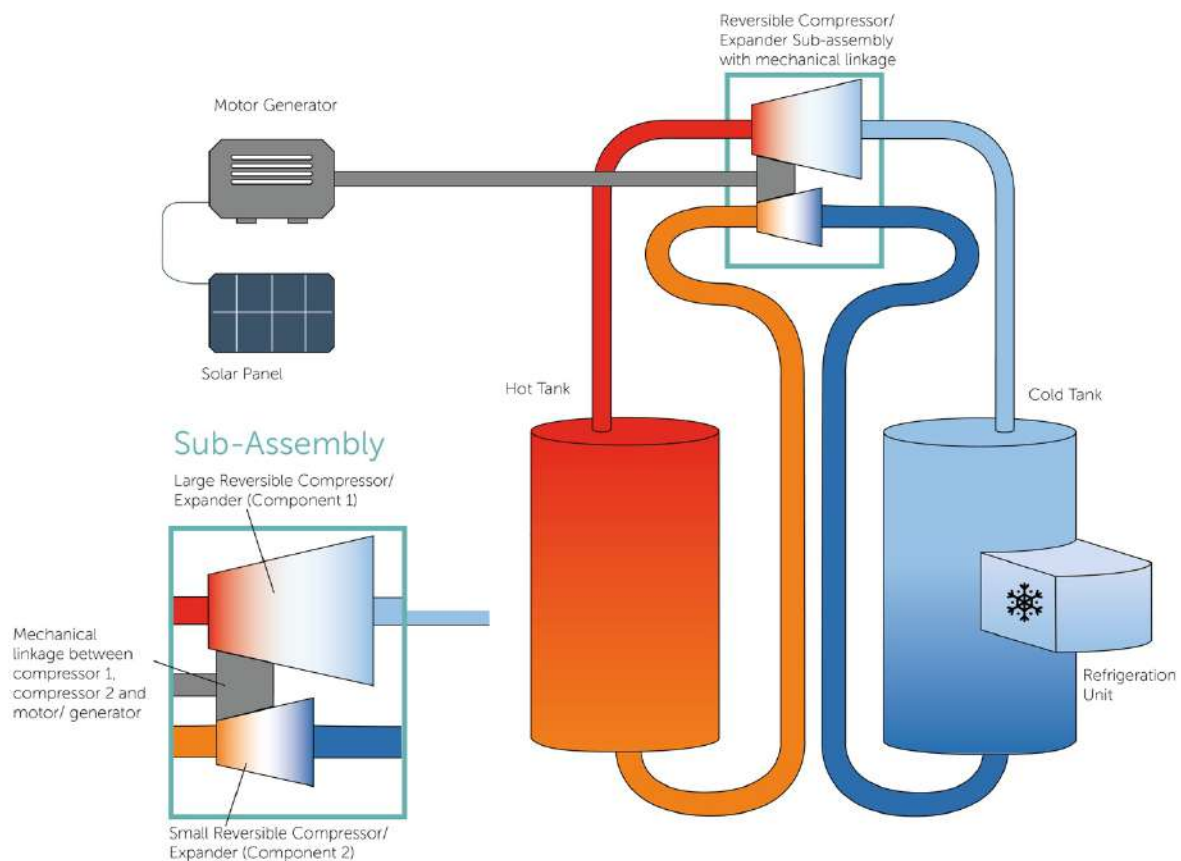


Figure 1: Product Architecture Diagram

The general system can be seen in Figure 1. A motor/generator is connected to a solar panel. During daylight hours the motor runs a compressor and an expander pumping Argon gas through two tanks. As the Argon it is compressed, it experiences a dramatic temperature rise. The heat generated is passed into a solid medium stored in the tanks, resulting in a net cooling of the Argon. The gas then passes through an expander, generating mechanical work resulting in a cooling of the Argon. As the working fluid passes through the cool tank it is heated by the solid medium. The result is a temperature increase in one tank and decrease in the other. At night, with no power input, the system naturally reverses with the temperature differential running the system, outputting mechanical work, which is used to turn the generator. If there is no power demand, output can be stopped with a proportional control valve [2].

Sub Assembly Requirements

This paper focuses on the reversible compressor/ expander sub assembly and the mechanical linkage between the large compressor, small compressor and motor/ generator. The system operates in two states, charging cycle and discharging cycle. The two compression expansion units are different sizes. This is critical to ensure that, when charging, more thermal energy is produced than mechanical work, and when discharging, more mechanical work is generated than thermal energy. For the duration of this paper, the large compressor/ expander will be referred to as component 1. The small compressor/ expander will be referred to as component 2.

Product Scoping

Alternative Uses for Hot and Cold Store

As discussed in a technical feasibility report [10], the thermal energy storage process lends itself to providing alternative uses for the hot and cold tanks. A variety of these uses were considered but those with most potential were refrigeration and cooking.

User Benefits for Additional Cooking Features

There are two primary areas which first-time electrical users would require the power for. Primary research conducted by Adkins et al (2012) [11] discusses these in detail and they are:

- Cooking and heating
- Lighting, Power for mobile phones, television and radio

As outlined by Adkins et al (2012) [11], rural communities without access to electricity rely primarily of wood as a fuel source for cooking and kerosene for light. The wood is sourced relatively cheaply as most is collected for free. Kerosene is expensive and as a result a disproportionate sum of a household's income is spent on lighting. This can be seen in figure 2.

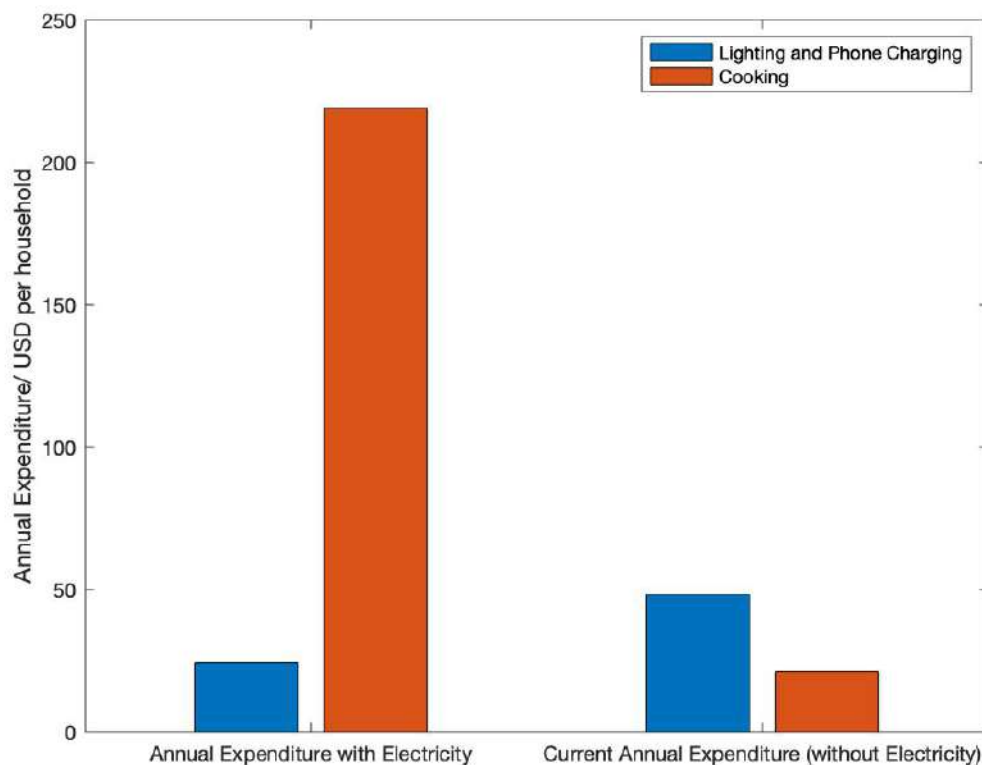


Figure 2: Annual Expenditure on Lighting and Cooking for Rural African Households and the Energy requirements for these processes

In order to examine the feasibility of PTES, the following assumptions have been made:

- Household average of 6 people [11]
- Use of three LED bulbs for 6 hours a day
- One hot meal a day, based on energy per capita [12].
- Each member of the household charges a phone for 1 hour
- Charge rate of \$0.40/kwh SSA average [13]

These figures were determined based on data from the Millennium Village Project (MVP), which was based on 10 villages throughout SSA that represented some of the poorest people in Africa and is therefore an accurate example of the target market of the proposed product.

Based on the financial distribution highlighted above, it was concluded that the PTES system scaling should be optimised to provide electricity to homes but not provide a source of cooking. The reason for this was twofold. Primarily, users could make a significant financial saving by switching to electrical lighting, the same could not be said for cooking. Secondly, by removing the cooking function, the product could be scaled up as it would not need to be kept in the home.

Refrigeration

Study by Sanni et al.[14] showed that families also stand to make financial savings with access to refrigeration. As shown in Figure 3

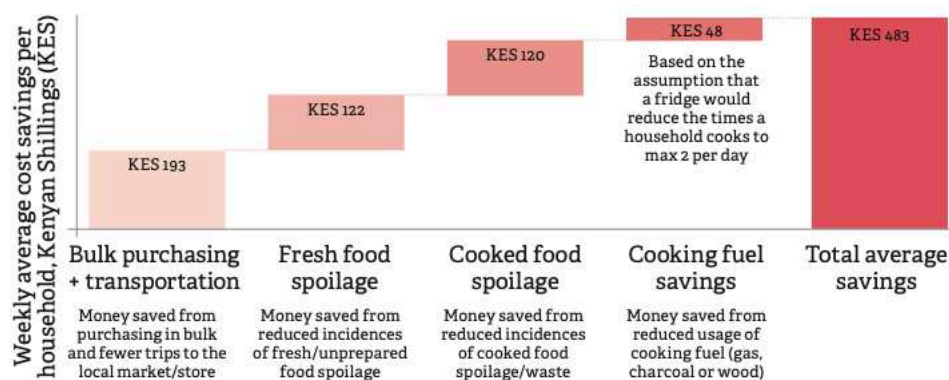


Figure 3: Savings due to Refrigeration access in Kenya [14]

When considering user needs in SSA countries it is essential to consider finances as this area has the highest percentage in the world of people living below the poverty line (41%) [15]. For this reason, it was concluded that the PTES system should provide lighting and refrigeration access as they can financially benefit the users.

Scaling Approximations

The initial development of the PTES system suggested its use on an industrial scale. However, development of this technology for rural an African environment required a scaling that fitted the needs of the users, whilst remaining technically feasible.

An essential consideration is accessibility. Research from PWC [16] showed that accessing rural communities in SSA can often only be achieved with 4-wheel-drive, off road vehicles. As a result, a maximum limit of 2m³ for the full system heating was determined. This was based on the bed size of a Toyota Hilux (most common truck in Africa [17]) and assuming a 2m tall cylindrical tank. (Appendix I)

Much of the literature on PTES systems suggests the efficiency of the system is closely linked to scale of the system [6]. This is logical as the rate of heat loss will be determined by the surface area/ volume ratio of the tanks. Given this assumption it was important to scale the system up as much as possible. With an upper limitation as mentioned above. However, this scaling is only possible if the user housing density is great enough to enable one system to easily provide for multiple households, as wiring and electrical pylon must be kept to a minimum. This is an important factor as data from Blimpo et al[18] shows that the cost associated with electrical pylons is non-trivial with average cost of approximately \$250/ pylon, across 10 African countries.

An average housing density for the target users was calculated. The method involved locating the 10 MVP villages on Google maps. Three optimum locations were then selected in each village. The number of buildings that could be accessed with 0, 1 and 2 pylons were determined. This was based on the need for a pylon every 50m. From these 30 locations, an average housing density was calculated. (Appendix I)

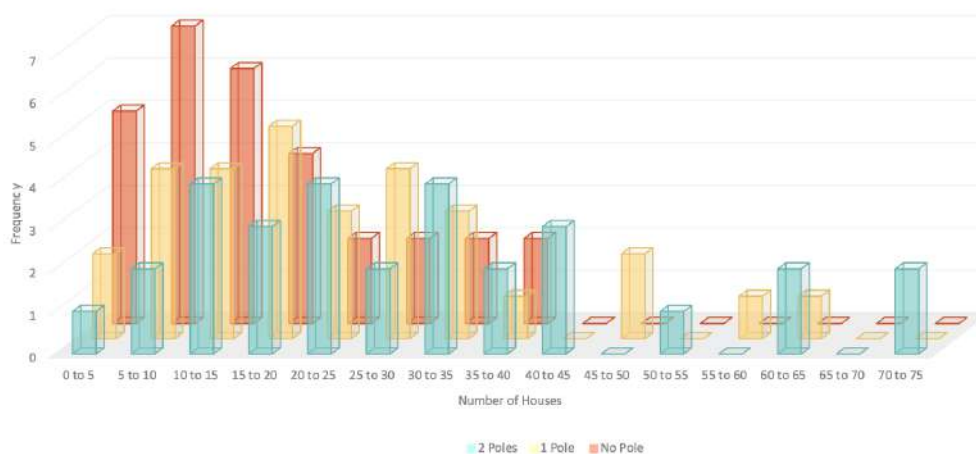


Figure 4: Housing Density in rural Africa

Figure 4 shows that the model housing density within a 50m radius is between 5 and 10 households.

			TIER 0	TIER 1	TIER 2	TIER 3	TIER 4	TIER 5	
Attributes	1	Peak capacity ratings (in W or daily Wh)		Min 3 W	Min 50 W	Min 200 W	Min 800 W	Min 2 kW	
				Min 12 Wh	Min 200 Wh	Min 1.0 kWh	Min 3.4 kWh	Min 8.2 kWh	
		OR services		Lighting of 1,000 lmhr/day	Electrical lighting, air circulation, television, and phone charging are possible				
	2	Availability (duration)	Hours per day	Min 4 hrs	Min 4 hrs	Min 8 hrs	Min 16 hrs	Min 23 hrs	
			Hours per evening	Min 1 hr	Min 2 hrs	Min 3 hrs	Min 4 hrs	Min 4 hrs	
	3	Reliability						Max 14 disruptions per week	Max 3 disruptions per week of total duration <2 hrs
	4	Quality						Voltage problems do not affect the use of desired appliances.	
	5	Legality						Bill is paid to the utility, prepaid cardseller, or authorized representative.	
	6	Health and safety						Absence of past accidents and perception of high risk in the future.	

Note: lmhr = lumen hours; kW = kilowatts; kWh = kilowatt hours; Max = maximum; Min = minimum; W = watts; Wh = watt hours.

Figure 5: Multi-tier frame work for electricity access[19]

Figure 5 shows the internationally accepted framework for electricity access, the required power output and daily energy usage to achieve each tier of electricity access per household.

As shown in Figure 2, the average household expenditure on lighting is approximately £50. Providing a Tier 3 level service would imply an annual usage of 365kWh, at US prices of \$0.13/ kWh (US average) this would imply an annual fee of \$47.50. Whether or not this pricing can be achieved remains to be seen, but it represents a good starting estimate.

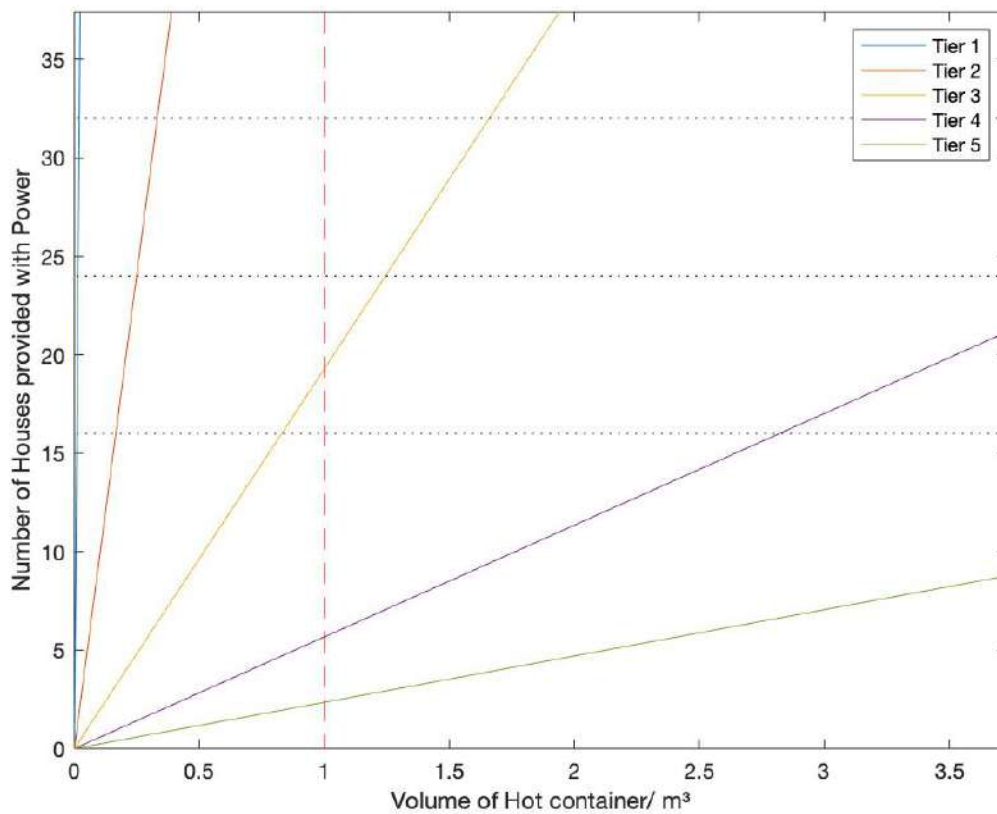


Figure 6: Households accessed at different tiers of electricity access

Early stage calculations of the energy capacity of the containers can be seen in Figure 6. This shows that a 2m³ system could provide electricity for 18 houses at Tier 3. This doesn't consider power requirements for refrigeration and so the real number is likely closer to the 5-10 houses, that could be targeted without need for pylons (Figure 4). Avoiding unnecessary costs and maintaining high efficiency.

Given the considerations discussed, it is reasonable to assume that there is a sufficient target market for a 2m³ system and that users will be able to afford the service provided as it is cheaper than their current lighting expenditure.

Sub-System: Reversible Compressor/ Expander with Mechanical Drive System

The critical requirement of the sub-assembly is to convert mechanical work to a temperature differential during the charging cycle and to reconvert that temperature differential to mechanical work during discharge. During the charge cycle, a motor powered by PV cells, turns component 1, while the working fluid is expanded through component 2. Work generated from this expansion is used to aid in the powering the compressor. When discharging, the fluid flow direction is reversed. Component 1 becomes the expander and generates output work which is used to power both component 2 in compression and the motor/ generator, outputting electricity from the system.

Through iterative modelling of the whole system (system integration report, [2]) it was determined that the optimum compression ratios, R_c for the components 1 and 2 are $R_c= 8$ and $R_c= 4$ respectively.

Scroll compressor/ expanders were selected as the optimum technology for use in the system for a variety of reasons, primarily simple reversibility (SG3 [20]). However, the required C_r for component 1 falls outside the optimum range for scroll compressor efficiency. As shown in Figure 7, isentropic efficiency peaks around $C_r = 2.5$ and decreases rapidly as the at C_r increases beyond 5.5.

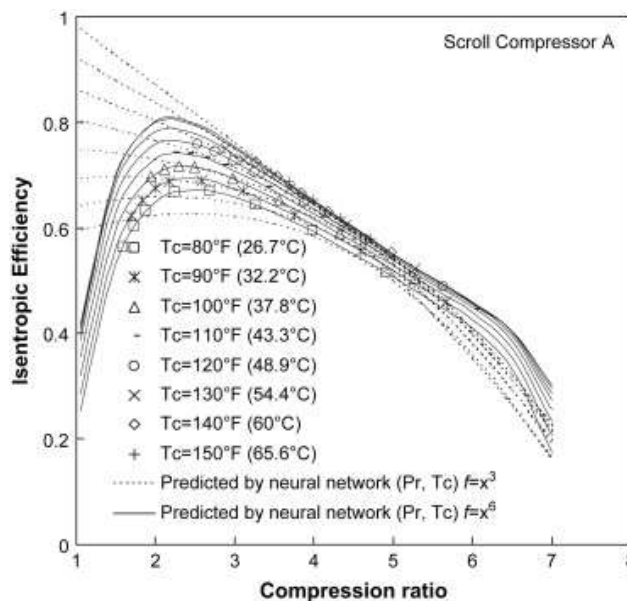


Figure 7: Isentropic efficiency of scroll compressors Varying with compression ratio [14]

In order to maintain an acceptable roundtrip efficiency, component 1 was designed as a two-stage system with one compressor $C_r = 4$ and the other $C_r = 2$.

Product Design Specification

Product Design Specification	Combined Scroll expansion and compression unit	Source	Requirement
Performance Requirements			
1.1 Product Life	The product has a target lifespan of 10 years	SG1 PDS	Essential
1.2 Operating speed	To maximise product life, the compressors should operate at low rotational velocity. <3000RPM	[24]	Essential
1.3 Input power range	The compressors are to be powered by a 4kw motor	System Intergration repo	Essential
1.4 Dual Function	Components must be able to function as both fluid compressors and expanders		Essential
1.5 Reversibility	System must be completely reversible whilst	PTES system design	Essential
1.6 Electrical Supply	Operate using 12/24v DC power	SG1 PDS	Essential
1.7 Output Power	Output power of 3kw to users	SG1 PDS	Essential
1.8 Efficiency	Operate at high efficiency >70%	SG1 PDS	
1.9 Pressure	Casings must be able to withstand pressures up	System Intergration repo	Essential
Operating Environment			
2.1 High Temperature operation	Function at temperatures up to 800degc	System Intergration repo	Essential
2.2 Maintenance	Given the remote location of the system operation location, the entire sub assembly should require infrequent maintenance. Maximum 2/ year	SG1 PDS	Essential
2.3 Fully Sealed Units	Product is to function in the field. To avoid contaminates that would increase wear, Components must be completely sealed		Essential
2.4 Countries of use	Components should be designed for users in the bottom 50 Human Development Index countries	SG1 PDS	Essential
Safety Requirements			
2.5 User Access	All moving parts must be covered to prevent user injury		Essential
2.6 Temperature	Warning signs to inform users of high temperature operation		Additional
Manufacturing			
2.7 Simplicity	Components should be simply designed to reduce assembly time		Additional
2.8 Cost	Cost effective materials should be used where ever possible		Additional
2.9 Use of the shelf components	Bespoke parts should be kept to a minimum wherever possible		Additional
Life Cycle			
3.1 End of Life	Components should be designed for ease of recycling or reuse wherever possible		Additional
3.2 End of Life	Components should be made of single material, not permanent bonding of separate materials.		Additional
3.3 Ease of repair	Components should be able to be repaired easily and cheaply		

Scroll Compressor Geometry

S_{fe}	<i>External Involute</i>
S_{fi}	<i>Internal Involute</i>
r_b	<i>involute basic circle radius</i>
φ	<i>Involute angle</i>
φ_{i0}	<i>Internal Involute Initial angle</i>
φ_{e0}	<i>External Involute Initial angle</i>
φ_{is}	<i>Internal Involute Starting angle</i>
φ_{es}	<i>External Involute Starting angle</i>
r_0	<i>Orbiting Radius</i>
r_c	<i>Interpolating Circle radius</i>
C_c	<i>Interpolating Circle</i>
O_c	<i>Interpolating Circle Origin</i>
θ	<i>Orbiting Angle</i>
φ_{max}	<i>End of Involute angle</i>
A_{dis}	<i>Discharge Area</i>
A_{suc}	<i>Suction Area</i>
V_{dis}	<i>Discharge Volume</i>
V_{suc}	<i>Suction Volume</i>
h	<i>Scroll Height</i>

Table 1: Nomenclature



Figure 8: Scroll compression process

The basic geometry of a scroll compressor is a pair of scrolls at an offset angle of π . One scroll is fixed in place whilst the other oscillates eccentrically which forms multiple chambers between the two scrolls. An opening allows for fluid flow into the scrolls (Figure 8). As the oscillation continues this opening is sealed fixing fluid mass in the chamber. As the contact points between the scrolls moves, the volume of the chambers reduce whilst remaining sealed, resulting in fluid compression. The fluid is forced to the centre of the scrolls where it exits through a discharge port at a higher pressure. In order to achieve expansion, the direction of rotation is reversed achieving the opposite effect.

Scroll Profile

The scroll profile is defined by two involutes¹ that are developed from a central circle, r_b . The geometry of the involutes are defined by an orthogonal frame (t,n) as outlined by Blunier et al. [21] eq 1-4.

$$t(\varphi) = (\text{Cos}\varphi, \quad \text{Sin}\varphi) \quad (1)$$

$$n(\varphi) = (-\text{Sin}\varphi, \quad \text{Cos}\varphi) \quad (2)$$

$$S_{fe}(r_b, \varphi_{e0}, \varphi) = r_b \cdot (t(\varphi) - (\varphi - \varphi_{e0}) \cdot n(\varphi)) \quad (3)$$

$$S_{fi}(r_b, \varphi_{i0}, \varphi) = r_b \cdot (t(\varphi) - (\varphi - \varphi_{i0}) \cdot n(\varphi)) \quad (4)$$

S_{fe} and S_{fi} describe the external and internal involutes of the scroll respectively. With the key variables being the initial angles of the internal and external involutes, φ_{i0} and φ_{e0} and the base circle, r_b (Figure 9). Where $t(\varphi)$ and $n(\varphi)$ represent the tangential and normal vectors to any point on the involutes. φ is the angle of rotation of any specific point on the scroll (Figure 10).

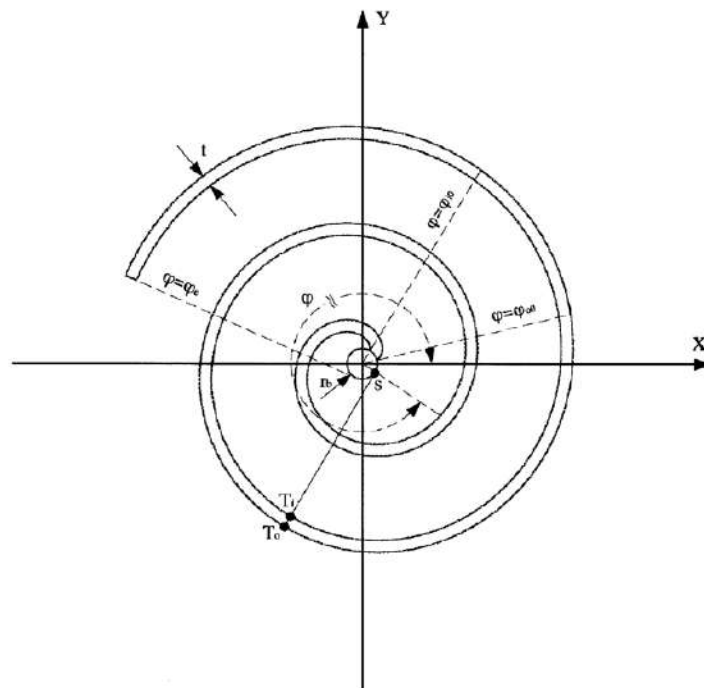


Figure 9: Geometrical Description of the Scroll Involute [22]

¹ Involute: The locus of a point considered as the end of a taut string being unwound from a given curve in the plane of that curve.

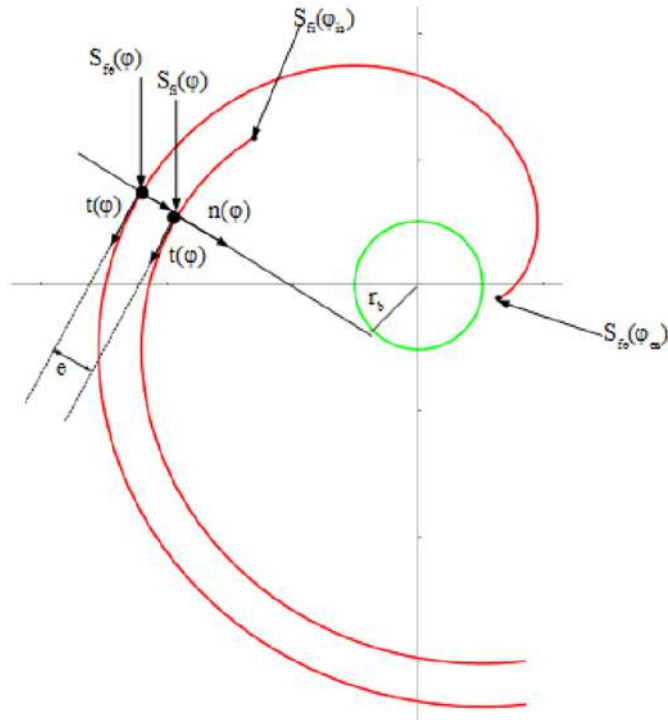


Figure 10: Tangential and Normal vectors to the Involute[23]

The orbital scroll shares the geometric profile of the fixed scroll but with an offset rotary transformation of π . The base circles of the two scrolls are offset by a distance r_0 .

$$r_0 = r_b (\varphi_{e0} - \varphi_{i0} + \pi) \tag{5}$$

Most geometric descriptions of scroll compressor units use the centre of the fixed scroll. However, the following modelling solution is based on a novel reference frame proposed by Wannassi et al. [23] whereby the scroll is modelled about an origin equidistant between the base circle of the fixed and orbiting scrolls. This increases the simplicity for geometric modelling (Figure 11).

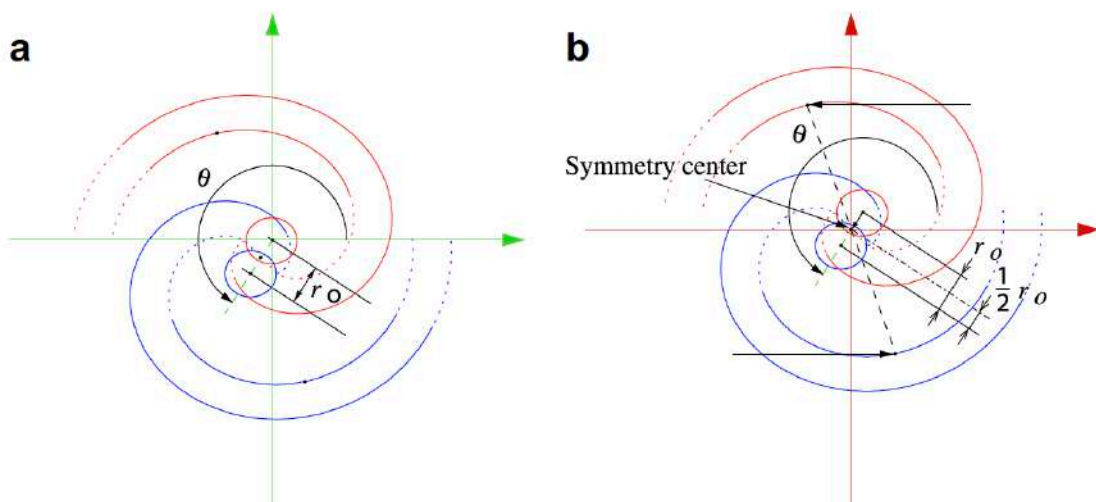


Figure 11: Novel Reference Frame Geometry [23]

Inner Scroll Profile Definition

The definition of the inner tip of the scrolls is an important consideration as it has a significant impact on the discharge volume and therefore the overall compression ratio of the compressor. Poor tip design can reduce flow rate due to partial blockage of the exit port which, in turn can lead to reduced power output when the unit is used for expansion. The design methodology used here follows that outlined by Blunier et al. [7] for single arc profiles. There are alternative methods such as that of the perfect meshing profile (PMP) [24][25]. PMPs are designs whereby the final internal volume is reduced to zero. These have some advantages; however, they do not lend themselves to simple revisability as the design requires valves to prevent blow back into the compressor chamber.

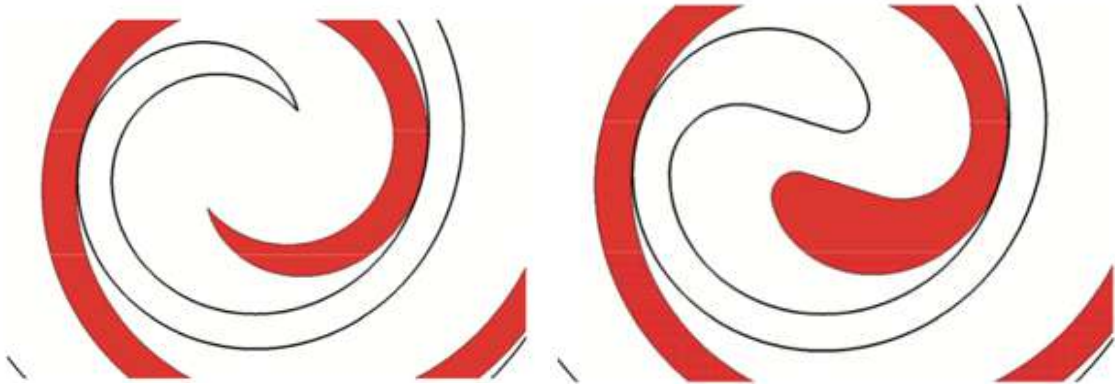


Figure 12: Single Arc and Perfect Mesh Tip Profiles [26]

Single Arc Tip Profile

The initial angles discussed above are the theoretical starting points of the scrolls. However, this design would not allow the orbital scroll to oscillate as required within the fixed scroll. Therefore, a real starting point must be found that allows complete rotation of the two scrolls without causing interference between scroll tips. The real starting points for internal and external Involutes are ϕ_{is} and ϕ_{es} .

The methodology presented by Blunier et al.[7] suggests connecting the starting points of the inner and outer scrolls with a circle, C_c as shown in Figure 13. The two key requirements for C_c are that it joins with ϕ_{is} without any discontinuity and that it passes through ϕ_{es} .

Given these two constraints the radius, r_c , and origin, O_c can be defined as:

$$r_c = \frac{r_b(2 + \xi_1^2 + \xi_2^2 - 2(1 + \xi_1\xi_2) \cdot \cos\xi_3 - 2(\xi_2 - \xi_1) \cdot \sin\xi_3)}{2(\xi_2 - \xi_1 \cdot \cos\xi_3 - \sin\xi_3)} \quad (6)$$

where

$$\xi_1 = \varphi_{es} - \varphi_{e0} \quad (7)$$

$$\xi_2 = \varphi_{is} - \varphi_{i0} \quad (8)$$

$$\xi_3 = \varphi_{is} - \varphi_{es} \quad (9)$$

Volume determination

A critical design feature of the scroll unit is that it has the correct compression ratio. This is defined by the suction volume and the discharge volume. These areas can be seen in Figure 14 with the suction volume equal to the sum of the white and purple suction chambers. The discharge volume is equal to the pink area multiplied by the height of the scroll.

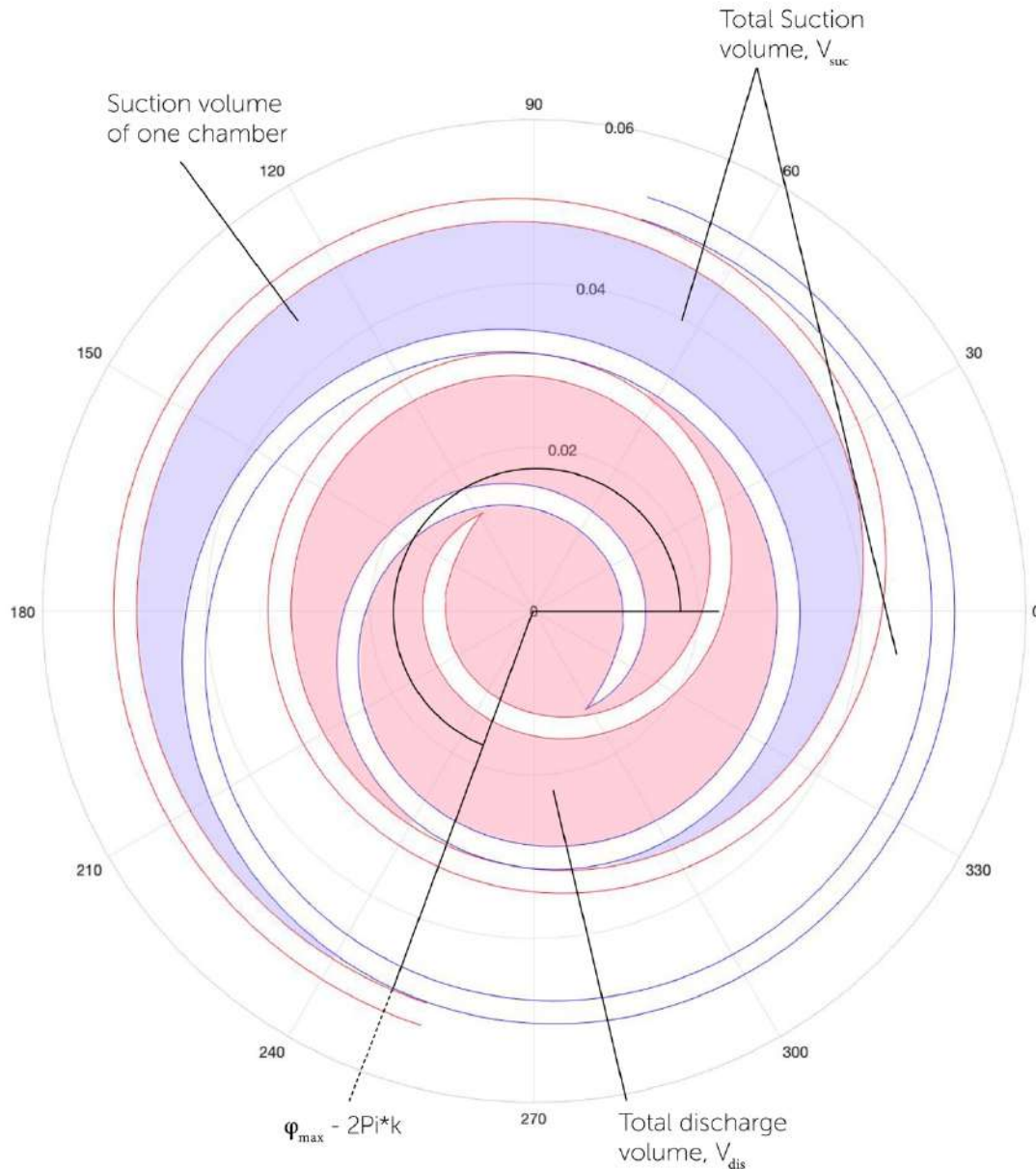


Figure 14: Suction and Discharge Volumes

Equation 11 shows the general expression for the area enclosed between two involutes, the full derivation of which can be found in Blunier et al. [7] ϕ_1 and ϕ_2 represents the two points of contact between the two scrolls.

$$f(\varphi_{y0}, \varphi_1, \varphi_2, \theta) = \frac{r_b^2}{3} \left((\varphi_2 - \varphi_{y0})^3 - (\varphi_1 - \varphi_{y0})^3 \right) - \frac{r_b r_0}{2} [\cos(\theta - \varphi_2) - \cos(\theta - \varphi_1) - (\varphi_2 - \varphi_{y0}) \sin(\theta - \varphi_2) + (\varphi_1 - \varphi_{y0}) \sin(\theta - \varphi_1)] \quad (11)$$

Assuming that the pressure in the chamber is equal to that outside the chamber whilst it is open, the point that defines the total suction volume of the outer chamber is when the gap between the scrolls closes, preventing any more fluid flow. The first point of contact between scrolls when the outer chamber closes is at ϕ_{max} , the outermost point of the scroll. Experimentation with the model showed that the contact point occurred when theta was out of phase with ϕ_{max} by $\pi/2$. Therefore, it can be concluded that the critical suction volume occurs when:

$$\theta = \phi_{max} - k \frac{\pi}{2} \quad (12)$$

where k is the number of rotations so that $0 < \theta < 2\pi$, θ is the oscillating angle of the orbital scroll.

$$V_{suc} = \frac{h}{2} (f(\phi_{i0}, \theta + 4\pi, \phi_{max}, \theta) - f(\phi_{e0}, \theta + 3\pi, \phi_{max} - \pi, \theta)) \quad (13)$$

at $\theta = \theta_{suc}$

The volume for the discharge volume is given by

$$V_{dis} = h(f(\phi_{i0}, \phi_{is}, \theta, \theta) - f(\phi_{e0}, \phi_{es}, \theta - \pi, \theta)) + V_{cl} \quad \text{at } \theta = \theta_{Dis} \quad (14)$$

$$V_{cl} = hr_c^2 \left(\pi - a \cdot \sin\left(\frac{2r_b}{r_c}\right) - \frac{2r_b}{r_c} \right) \quad (15)$$

Where V_{cl} is the clearance volume, i.e. the volume contained in the centre of the scroll before contact is lost between the scroll tip and the wall of the opposite scroll. [27]

$\theta = \theta_{dis}$ as it's the point at which discharge starts.

By using these equations for suction and discharge volumes, a scroll profile with the correct compression ratio could be modelled.

Design Optimisation of Scroll Profile

Input Parameters

In order to define the profile for the scrolls, a MATLAB model was developed. The primary challenge when considering how to implement the model was the large number of potential variables. The geometry of the scroll can be fully defined by the variables r_b , ϕ_{i0} , ϕ_{e0} , ϕ_{is} , ϕ_{es} , h and ϕ_{max} as described above.

As outlined in the system integration report [2], the target volumes for input and output of each compressor were outlined based on equal mass flow rate through each unit. From this volumetric flow rates were determined.

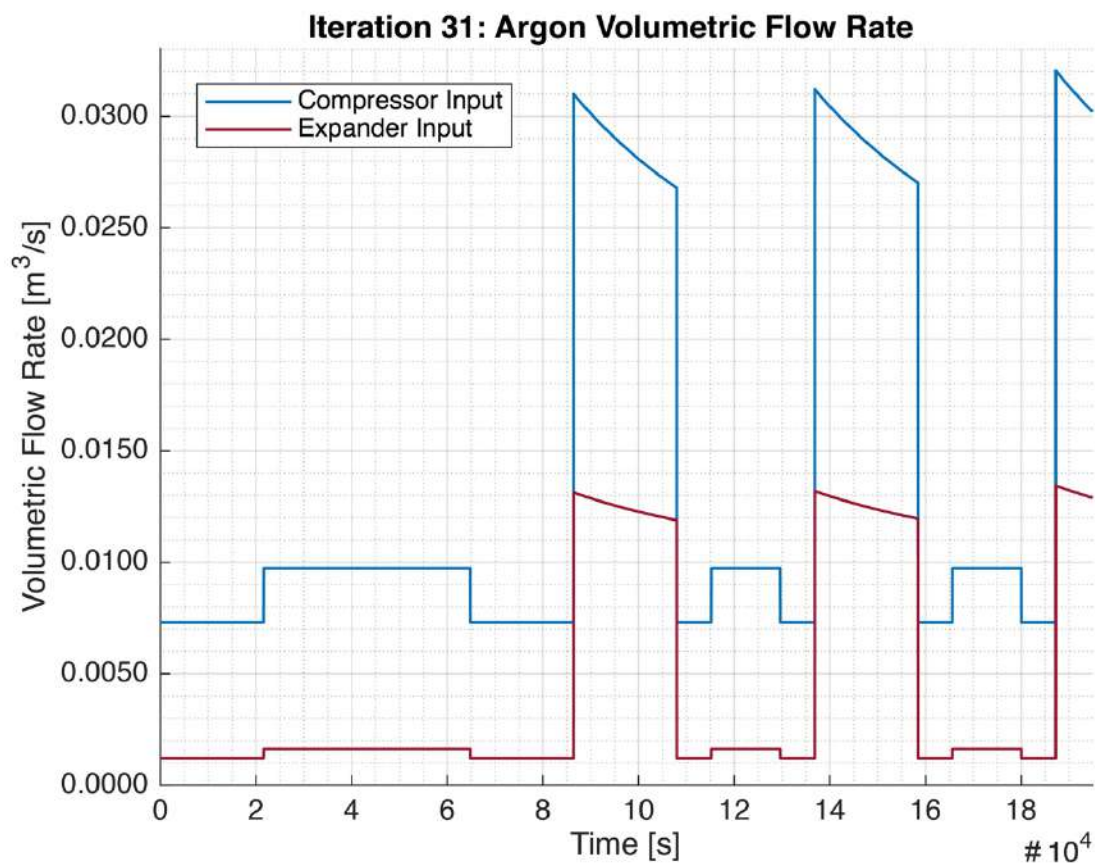


Figure 15: Volumetric flow rates through Compressor and Expander [2]

This gives an input into the system of volumetric flow rate and compression ratio. From these parameters the discharge volumes could be simply calculated. The process used for defining the core parameters from these input volumes can be seen in the flow diagram, Figure 16.

Software Flow Diagram

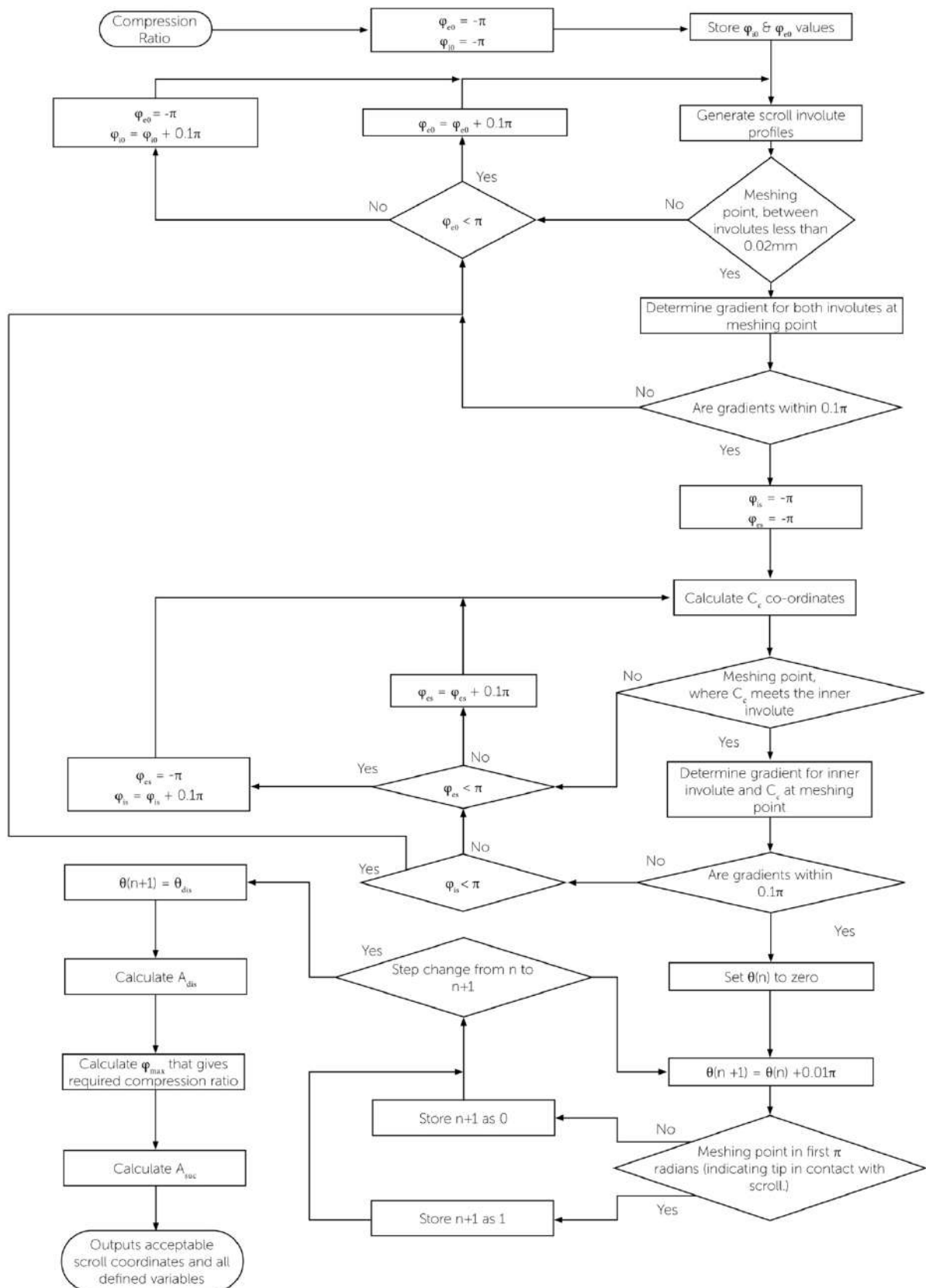


Figure 16: Software Flow diagram for Scroll Profile Optimisation

Optimisation Sequence Methodology

Preliminary calculations were carried out to find an approximate value for initial circle radius, r_b that gave an appropriate discharge area. It was determined that an acceptable range for r_b , which defines the involutes was $2\text{ mm} < r_b < 5\text{ mm}$.

1. Initial angles, ϕ_{i0} and ϕ_{e0} , were both set to minus π .
2. Involute for the scroll were generated using these values.

From these two variables, many possible involutes could be generated however the vast majority do not comply with the required geometry of the scroll. The two scrolls are required to mesh together to within a range 0.02 mm [28][29]. In order to properly form the compression/ expansion chambers with minimal radial leakage between chambers.

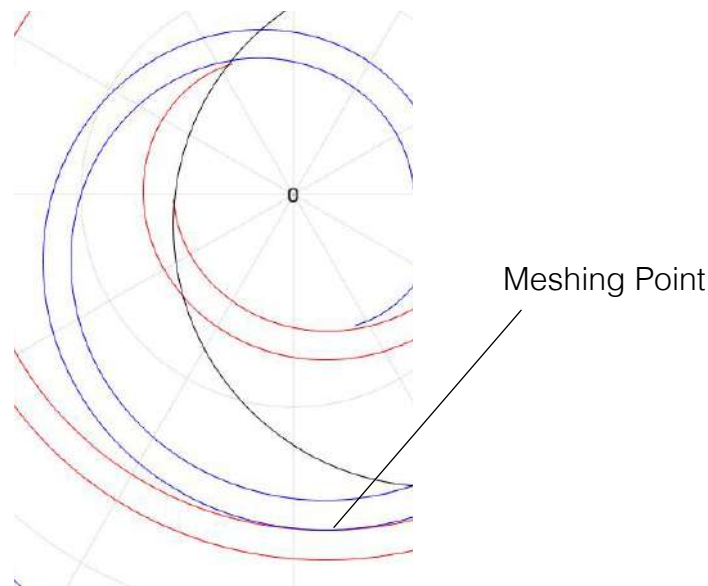


Figure 17: Scroll Profile Meshing Point

3. Polar coordinates were determined for a single meshing point (where the internal involute of one scroll meets the external involute of the other scroll). If there was no meshing point initial angle, ϕ_{e0} would increase by step of 0.1π radians.
4. If a meshing point within 0.02 mm was found, the Gradient was then determined at the point for both scrolls. The involutes must have the same gradient at the meshing point to ensure they do not cross each other. If gradients were within a tolerance of 0.05 mm , the initial angles were considered acceptable.
5. For acceptable initial angles, a similar process was completed to find starting angles that intersected correctly with the tip defining arc made by circle C_c .

Correct intersection occurs when the circle meets the inner involute tangentially and also crosses the outer involute line.

In order to determine the discharge area of the generated scroll profile, the angle, θ_{dis} , at which the discharge chamber opens to the discharge port had to be calculated. This occurs when the tip of the scrolls loose contact with the inner face of the other scroll (Figure 18, far right).



Figure 18: Scroll movement with variable θ

Figure 18 shows the progression of the orbital scroll as theta changes

6. To calculate the discharge area, θ was set to an arbitrary value of $\theta = 0$. Once again, the same method of determine whether there was intersection between involutes was used, though without the stipulation that the gradients be similar, but with a limitation of the first pi radians of rotation. This ensured only the tip interaction with the other scroll was considered.
7. If there was a meshing point, theta was stored in a binary matrix = 1. If no interaction occurred, a value of zero was stored.
8. This was repeated, with small increases in theta until the binary matrix experienced a step change. At this value of theta, the tip of the scroll is either making or losing contact with the internal involute of the other scroll. Defining theta as the point of discharge, $\theta = \theta_{dis}$.
9. This value of theta was then used to calculate the discharge area, A_{dis} . (equation 13)
10. Equation 12 was then used to determine the ϕ_{max} value where $A_{dis} = A_{dis} * C_r$ (required compression ratio)

Though requiring a large amount of computing power, this was deemed the most robust approach as there is limited documented research regarding recommended starting points for the defining variables. Other sorting methods (such as shooter methods) were unable to perform effectively given the number of variables.

Optimisation of Scroll Height and Operating Speed

Having defined the geometry of the scroll profile, the height of the scroll had to be determined. Two considerations were used to achieve this.

- Recommended practice that the ratio of inner circle to scroll height r_b/h fall in the range 0.09-0.013. [30]
- Recommended practice for long lived, oil free scroll compressor to operate in a range below 2500 rpm [31]

These ranges were used to find a scroll height that produced the required volumetric flow rate with acceptable operating speed.

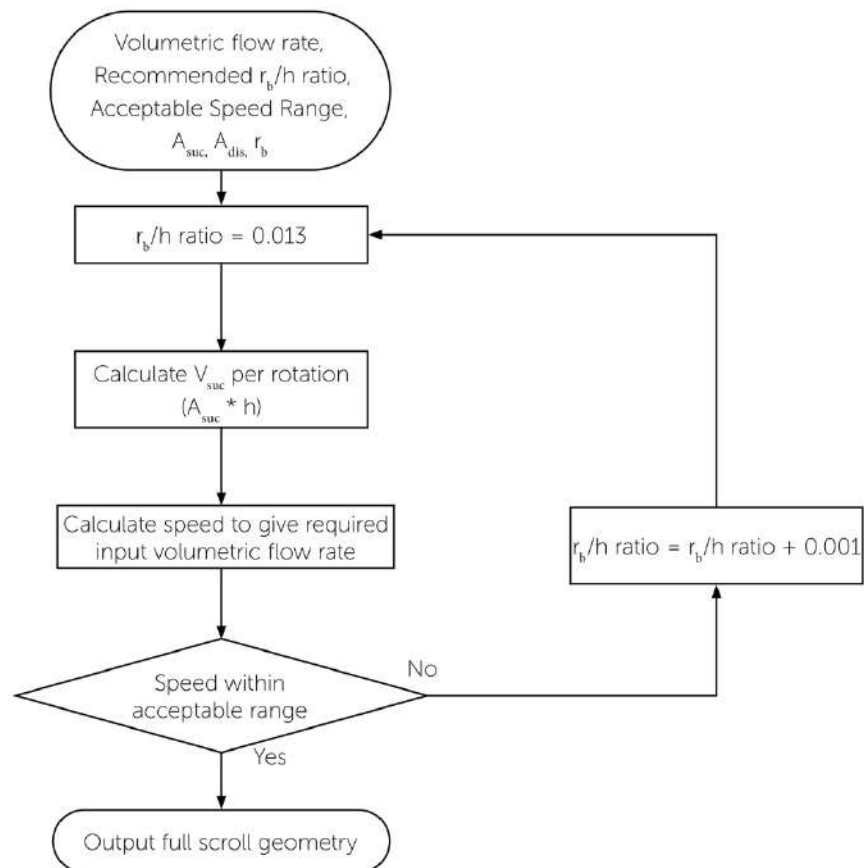


Figure 19: Rotational Speed and Scroll Height Optimisation

Scroll Volume Validation

The software outlined in Figure 16 and Figure 19 were performed on an iterative basis until a full scroll profile was developed that met all the specification requirements.

In order to guarantee the process had worked correctly, a quantitative volume validation was performed. This involved exporting the cartesian coordinates stored in the MATLAB model, into Fusion 360. This allowed the suction and discharge areas to be verified. The input volumetric flow rate was then calculated manually using the output height and rotational speed from Figure 19. These results were then compared with the maximum volumetric flow rates for component 1 and 2 in both charge and discharge cycles (see Figure 15).

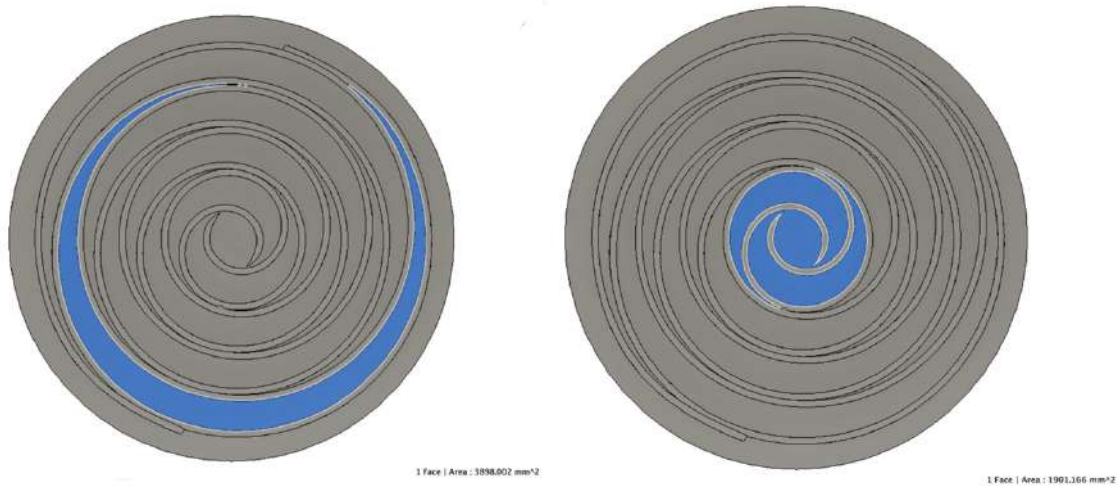


Figure 20: Manual verification of suction and discharge areas using Fusion360

r_b	3mm
φ_{i0}	0.9425 rad
φ_{e0}	0 rad
φ_{is}	4.7224 rad
φ_{es}	3.7699 rad
r_0	6.60 mm
r_c	24.63 mm
φ_{max}	30.82 rad
A_{dis}	1900mm ²
A_{suc}	7600mm ²
V_{dis}	190,000mm ³
V_{suc}	760,000mm ³
h	0.1m
r_b/h	0.03

Table 2: Scroll Profile Parameters

Product Requirement Specification

Having defined the geometry of the scroll profile, a detailed requirement specification was developed for the full mechanical system.

Requirement Specification	Component 1	Component 2	Source
Fluid Considerations			
Compression ratio	8	4	Full system Model
Volumetric Flow rate (m ³ /s)			
Charge Cycle	0.01	0.002	Full system Model
Discharge Cycle	0.031	0.013	
Area of Discharge chamber			
Fluid linkage	piping is required for flow in/ out of both		
Base Circle to Height ratio (r_b/h)	0.09- 0.013		Oralli et al. (2011)
Scroll Profile			
Discharge Area of compressor/ mm ²	1900		
Height of Scroll/ mm			
Stage 1	10	5	
Stage 2	5	-	Calculated through scroll modelling
Discharge Volume/ mm ³			
Stage 1	190000	95000	
Stage 2	95000	-	
Suction Volume/ mm ³	760000	380000	
Mechanical			
Maximum Rotary speed (RPM)	3000		Oralli et al. (2011)
Discharge cycle speed	2400	2000	Calculated through scroll modelling
Charge Cycle speed	800	315	
Motor/ Generator			
Output Power/ W	4000		
Operating Efficiency/ %	92		VolcanoMotors [15]
Operating Voltage/ V	48		
Operating load/ A	90.6		
Rated Speed/ RPM	2580		
Gear Ratio	Charge Cycle	Discharge Cycle	
Motor/ Component 1/ Component 2	1:3.225:9.675	0.9:1:1.2	

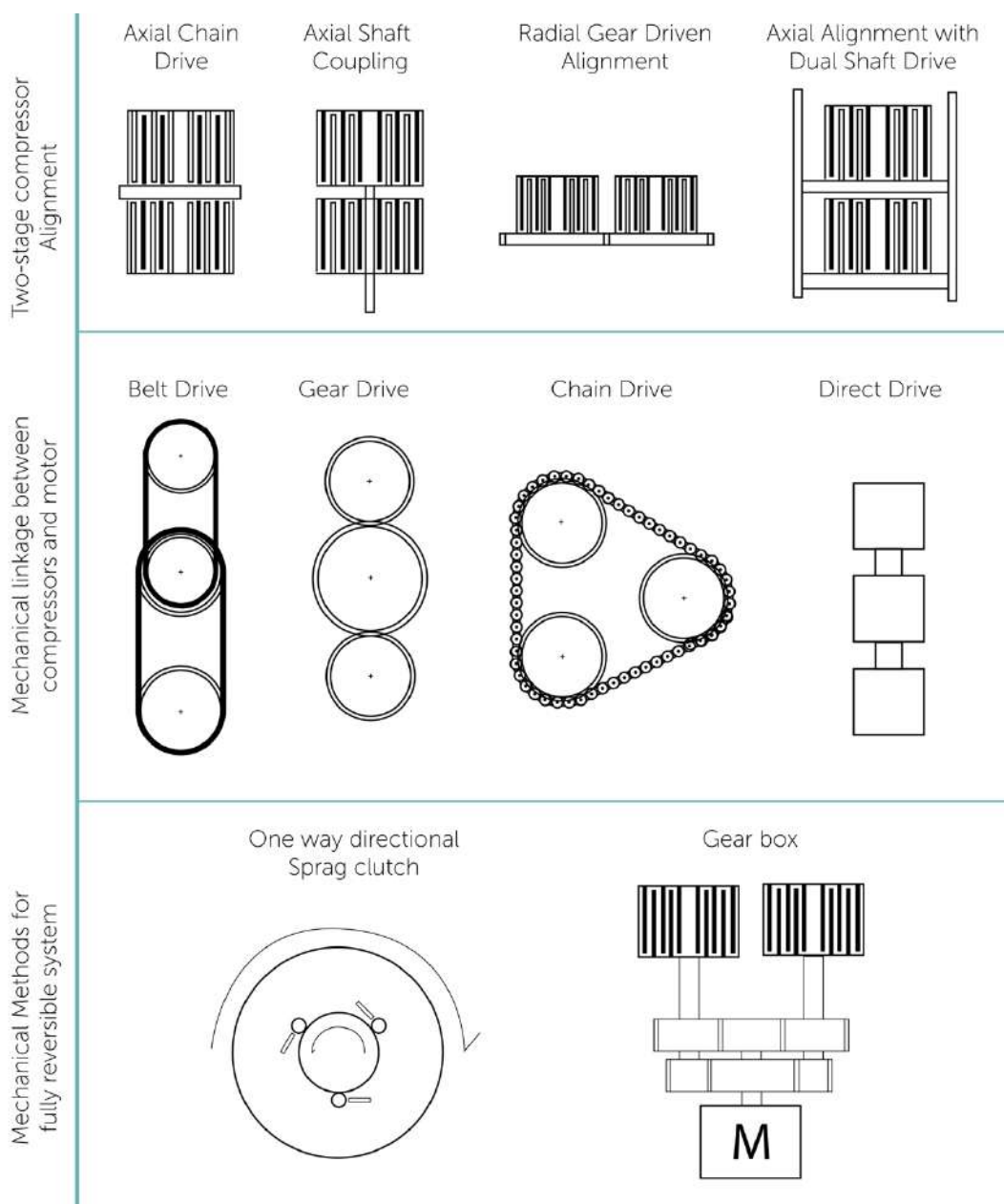
Figure 21: Requirement Specification

Initial Concept Design

As previously outlined, component 1 was comprised of two lower compression units in order to ensure high operating efficiency. However, this presented new design complexity. Possible arrangements were considered in a morphological chart. The three primary design operation functions in the sub-assembly were:

- Mechanical arrangement of the two stage scroll compressor
- Mechanical linkage between components 1, 2 and motor
- Geared reversibility

Morphological Chart



Controlled Convergence

Each of the possible design methods was analysed and then compared using a controlled convergence method based on key requirements for each operating function.

Two Scroll Arrangement

Reverse axial coupling: This arrangement would consist of two orbiting scrolls connected to the same central plate with fixed scrolls connected above and below. The advantage of this being that a single mechanical drive system can operate both scrolls. However, as the fluid flows into the unit at the side and out of the centre, the gas would then need to be directed around the housing of the first scroll to reach the second.

Axial Coupling: A direct axial coupling could be used to drive both scrolls. This is also simple in terms of mechanical drive. However, the complexity of the scroll profile is increased as it need to incorporate a shaft running through the first fixed scroll in order to reach the second.

Radial alignment with gear drive: Radial Alignment avoids fluid flow complications but the need for mechanical gearing would reduce the efficiency for the driven scroll.

Duel shaft axial alignment: This design allows for simplification of the fluid flow path without the increased complexity to the scroll profile of a direct drive shaft through the scroll. Mechanical efficiency losses are also avoided as there is no requirement for gearing.

	Fluid Flow Simplicity	Mechanical Losses	Scroll Simplicity	Mechanical Simplicity	Total
Reverse axial coupling	Datum				0
Axial Coupling	+1	+1	-2	+1	+1
Radial alignment with gear drive	0	-1	0	-1	-2
Duel shaft axial alignment	+1	+1	0	0	+2

Mechanical Linkage	Efficiency	Maintenance Requirements	Scroll Simplicity	Total
Belt drive	Datum			0
Chain Drive	-1	-1	0	-2
Direct gear Drive	-1	-1	0	-2
Straight Drive Shaft	+1	+1	-2	0

Geared Reversibility

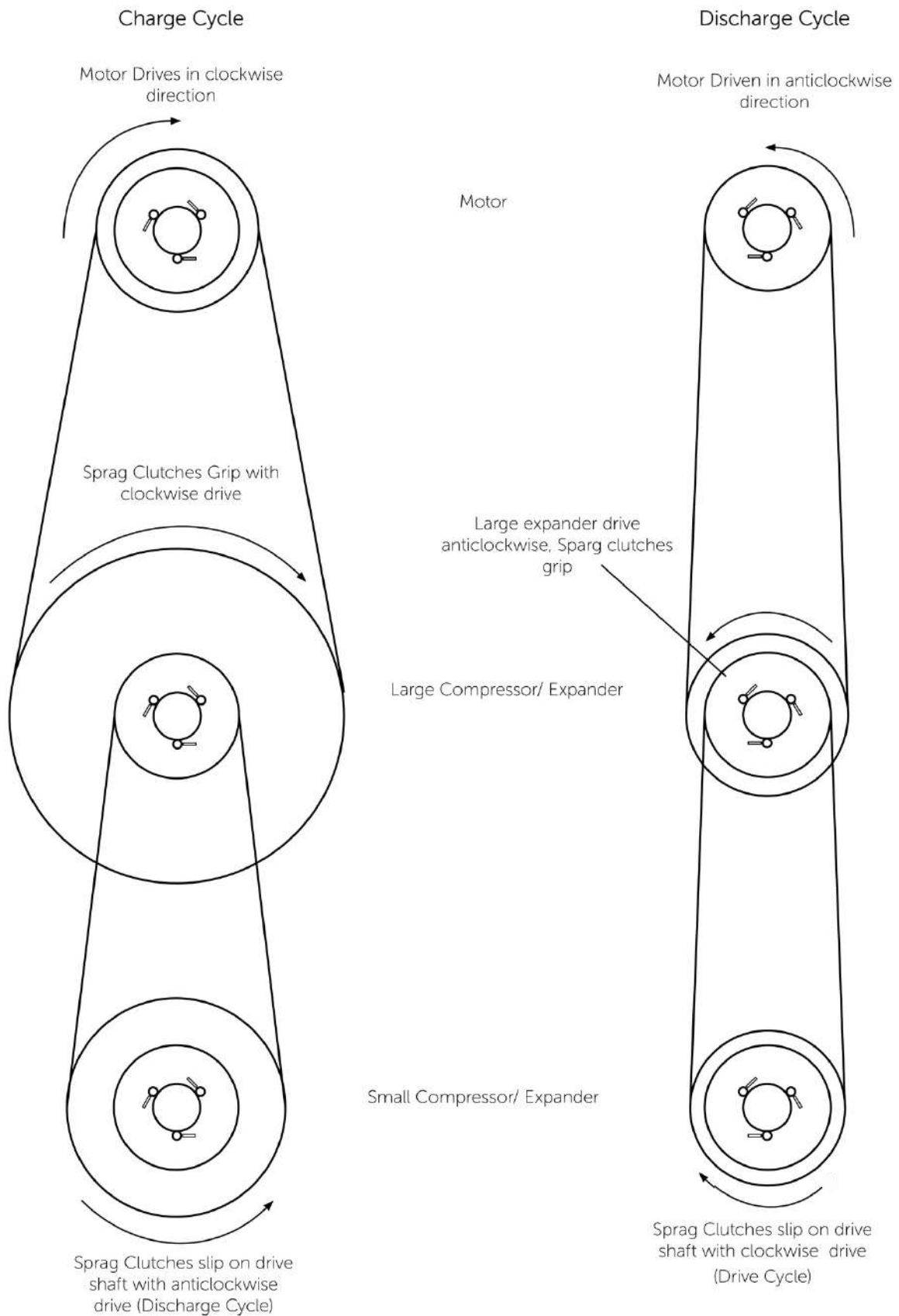
The rotational speed ratio between component 1, 2 and the motor/ generator changes from the charge cycle to discharge cycle (see requirement spec). Therefore, a gear change is required when the system flips from charging to discharging.

Gearbox: The most common solution for changing rotational speed ratios. Offers a simple and compact gearing method. Gear changes either require manual transmission or integration of an electrical component to achieve automatic transmission. It would also need oil, increasing the maintenance requirements.

Sprag Clutch: A component that rotates on the shaft when driven in one direction. However, when rotation is reversed, the shaft spins independently of the clutch system. This could be integrated with different sizes of gear/pulley system so that reversal of the rotation direction could automatically adjust the gearing of the system.

	Automatic Operation	Oil free operation	Maintenance requirements	Design Simplicity	Total
Gearbox	Datum				0
Sprag Clutch	+1	+1	0	-1	+1

Concept Design: Full mechanical Linkage system - Sprag clutch



Design Embodiment

The following section outlines some of the key considerations made during the detailed design process, which was carried out with constant consideration of the three key principles of design embodiment.

Clarity
Simplicity
Safety

The methodology used follows the flow diagram outlined in Figure 22

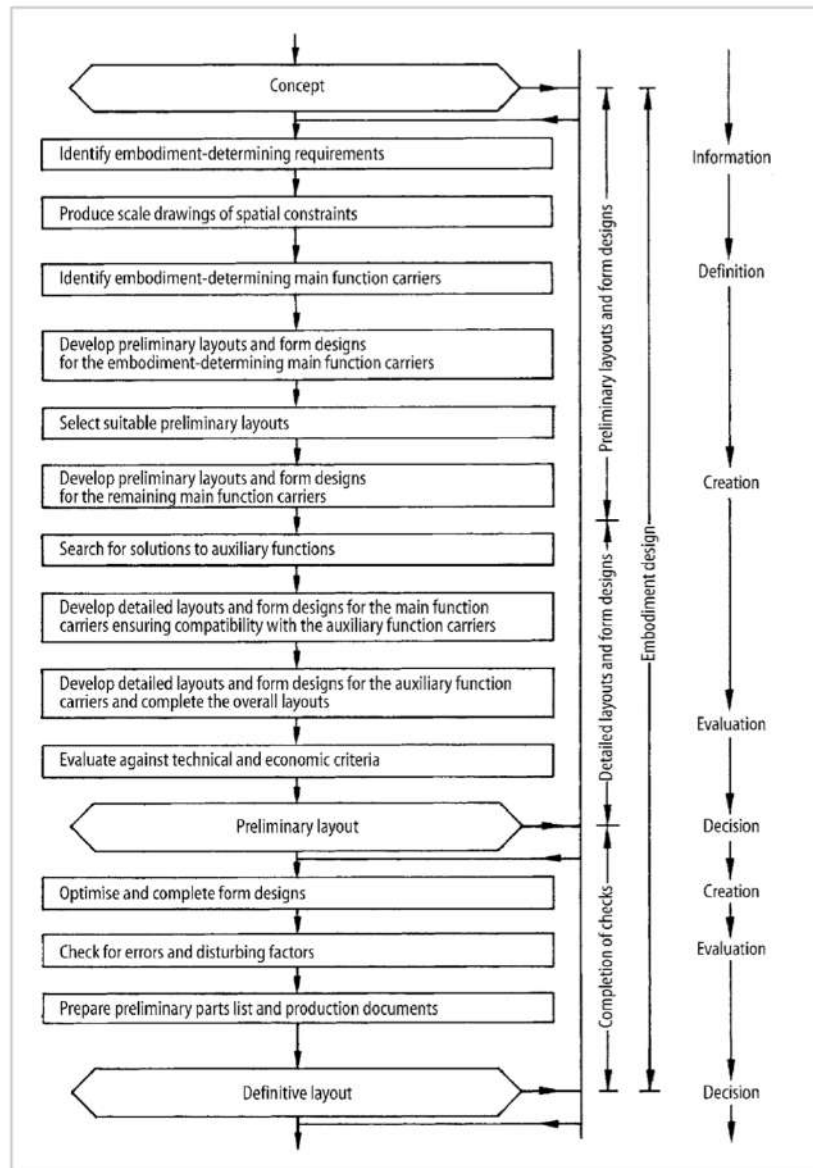


Figure 22: Design Embodiment process[32]

Compressor/ Expander 1

Component 1 used a two-stage compression process. In order to achieve a compression ratio of 8, the first stage has $Cr = 4$ and the second, $Cr = 2$. The primary considerations for this unit were:

- The fixed scrolls oscillate at a radius R_b
- Both scrolls have the same rotational speed
- Fluid flows correctly through the first scroll then the second.
- No fluid can escape the unit
- Scrolls follow a fixed path

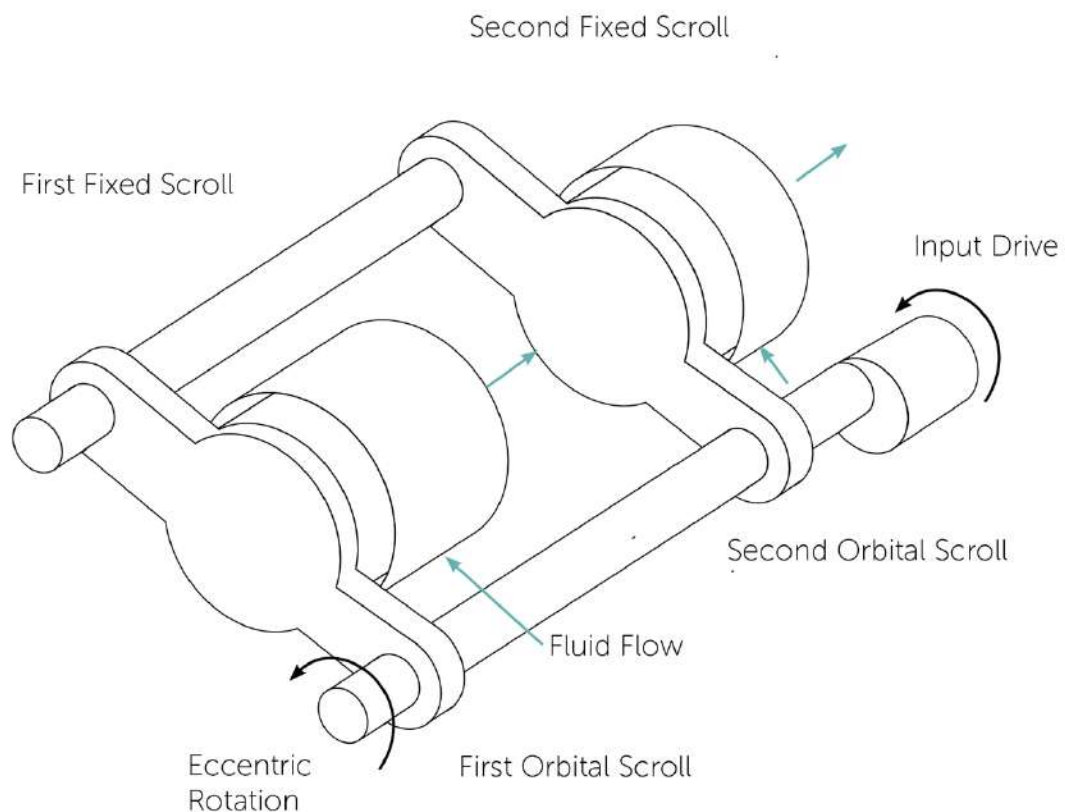


Figure 23: Preliminary layout and primary requirements of the two-stage scroll compressor

Housing Design

This basic design layout was developed using a linear arrangement with four housing bodies. Two housings for the fixed scroll units and a housing cover for each fixed scroll. (see eCOOL_SJRW_B1(A-D) & eCOOL_SJRW_B1_EXP). The linear arrangement allows for simple assembly of components with eight housing assembly rods to establish proper alignment. The simple assembly process will reduce the assembly time leading to manufacturing overheads.

Shaft Design

The shaft design consists of a drive shaft and a driven shaft that ensures the scrolls follow the correct orbital path. This guarantees contact is maintained between the fixed and orbital scrolls at all times, which is critical for proper compression of the working fluid. Both shafts are fully constrained by bearings in the outermost housing parts (eCOOL_SJRW_014 & eCOOL_SJRW_015). This positioning provides support either side of the eccentric section of the shafts. Sealed single row deep groove ball bearings were selected as they experience low friction leading to long operational life and low maintenance. They can carry high radial loads which will be required both due to the eccentricity of the shaft and the load provided by the pulley assembly (see eCOOL_SJRW_B3). Internal shaft thicknesses were determined using torque calculations (appendix III). The external shaft thickness was defined by the pulley selection [33]. The orbital scrolls were located on the shaft using cylindrical roller bearings, which also handle radial loads well and have accurate axial alignment. Accurate axial alignment is essential as the separation between fixed and orbital scrolls directly affects axial leakage between compression chambers.

Counterweights were integrated in between rotating scrolls to counteract the radial forces induced by the eccentric shaft which will reduce radial loads experienced by all bearings and increase the product life span. The counterweights were located with keys/keyways to ISO standards [34]. Orbital scrolls and counterweights were all axially located using washers and circlips. This will make assembly simple, reducing assembly time. The evenly weighted shaft should also reduce maintenance costs as it increases design reliability.

Special design consideration was given to the step from aligned to eccentric shaft (see eCOOL_SJRW_20 by datum point C). All points on the step have a diameter less than 25mm (the diameter of eccentric shaft) and the separation between the step down and the start of the eccentric shaft is well over the 18mm width of the orbital scroll roller bearing to ensure it can be properly assembled and located on the eccentric shaft without interference.

Thrust Roller Ball Bearings

The accurate location of the orbital scroll is controlled by the thrust roller ball bearings located between the orbital scroll and the housing cover (see eCOOL_SJRW_B1 H, I). These are axially aligned with the orbital scroll and so will prevent axial movement away from the fixed scroll which could lead to fluid escaping the compression chambers. These ball bearings are free to rotate, contained by two plates located on the orbital scroll and housing cover (see eCOOL_SJRW_B1 A). This allows for freedom of radial movement as the orbital scroll oscillates [35].

Fluid Flow

The working fluid inlet port is located on the side of the first compression chamber. The working fluid is drawn in and compressed as it moves toward the centre of the first scroll pair where it exits into the second scroll housing cover. The working fluid is prevented from escaping the first compression chamber by the top of the orbital scroll, which forms a rolling seal with the recessed face of the fixed scroll housing

cover (see eCOOL_SJRW_B1 J). After exiting the first compression chamber, the working fluid flows into the second compression chamber through holes in the orbital scroll top (see eCOOL_SJRW_B1 G). As the fluid has already been compressed to a $Cr = 4$ by the first scroll, the second scroll only needs to achieve a compression ratio of 2 to achieve the desired total of 8. Rather than use a different scroll profile, the same scroll has been used in the second chamber. This will allow the same mould pattern to be used to cast both scroll. This will reduce the manufacturing complexity and reduce cost. In order to reduce the compression ratio from 4 to 2 in the second compression chamber, 2 mm breather holes will be drilled into the top of the orbital scroll. By locating these holes just outside the scroll profile, they allow fluid flow out of one of the scroll intakes whilst keeping the other intake path completely sealed. This effectively drops the compression ratio of the second scroll from 4 to 2. The sealed chamber functions as usual, compressing the fluid to the centre where it exits the unit through a second discharge port. Using the same scroll profile also simplifies the shaft design as both scrolls oscillate with the same eccentricity.

Dust Cover and Seal

A dust cover and seal were fitted where the drive shaft enters the First scroll housing, this is to prevent impurities from entering what is otherwise a closed system. It also prevents any fluid leakage from escaping the housing

Compressor/ Expander 2

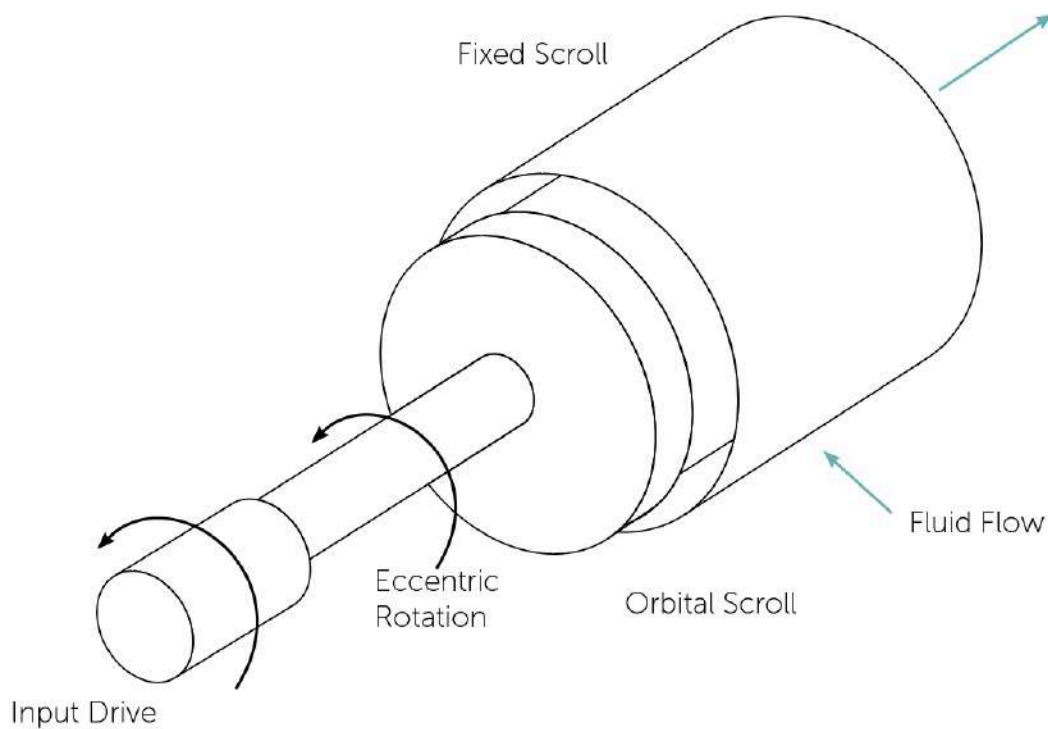


Figure 24: Preliminary layout and Basic Requirements of the Single-stage scroll compressor

The general design of the single stage compressor follows similar principles to that of the two-stage compressor. Instead of a dual shaft design, the orbital scroll is driven by a single drive shaft with eccentric attachment via a cylindrical roller bearing. The same standard components have been used wherever possible, including the main deep groove ball bearing, cylindrical roller bearing and shaft circlips. This is to simplify the manufacturing and assembly process.

Both the single-stage and two-stage units are based on an oil free design to reduce maintenance requirements. The use of oil-free scroll compressors is well documented and is the industry standard for high temperature units such as these [36]. (For detailed design see eCOOL_SJRW_B1 & 36).

Mechanical Linkage

Sprag Clutches

The fundamental component to the reversible pulley assembly is the sprag clutch, as described in the controlled convergence. (see eCOOL_SJRW_B3 B, D) The sprag clutch consists of a body that loosely locates on the shaft. Three cylindrical rollers are constrained in a notch in the body. If the shaft rotates clockwise, the rollers will catch between the notch and the shaft, causing the sprag clutch body to rotate. However, when the shaft rotation is reversed, the rollers are free to move and the clutch spins freely on the shaft. By integrating these clutches directly onto the pulleys, the direction of system rotation defines which set of pulleys is being used to drive the system, whilst the other will spin freely transferring no torque.

Belts and pulleys

These were all sourced from the Fenner catalogue using torque calculations to define the requirements. Direct drive was used between components. This was required to enable the vertical alignment which was required for the most efficient assembly of the full system [2]. The linear arrangement with belts all on one side ensure that they are easily accessible, as the belts are the first component that will require replacement.

Tensioners

Belt tensioners were used for the v-belts between the two compressor/ expander units. They were not deemed necessary between the two-stage unit and the motor, as the belts are much shorter, and the large belts are likely to need replacing before the smaller ones have stretched beyond acceptable limits. Both tensioners are spring loaded to remove the requirement for manual adjustment.

Motor Selection

A DC brushless motor/ generator was selected as they have the highest efficiency of DC motors [37]. This selection was based on an input power of 4kW as that is the peak power demand of the system [2], (see requirements spec). DC brushless motors can also be used as efficient electrical generators as they have fixed permanent magnets, which also reducing friction and other losses. Using a motor/ generator will result in a simpler mechanical system, reduce parts, costs and assembly time. Voltage was also considered during this selection as a low voltage motor was required in order to operate effectively using 24V solar panels as a power source.

Material Selection

All components without critical material properties such as washers were made of cheap, low quality steel (EN1A). However, for essential, functioning components such as the scroll profiles and shafts, compromises were not made of materials to reduce cost. It was considered more important to ensure longevity of design. The proposed business plan [9], is to run this business as a service. This results in the company assuming responsibility of maintenance costs. Therefore, in the long run, it makes

more financial sense to make a long-lasting product than to save costs by sacrificing material quality.

Failure Analysis: Trouble Tree

The full sub-system was analysed for potential failures using a trouble tree

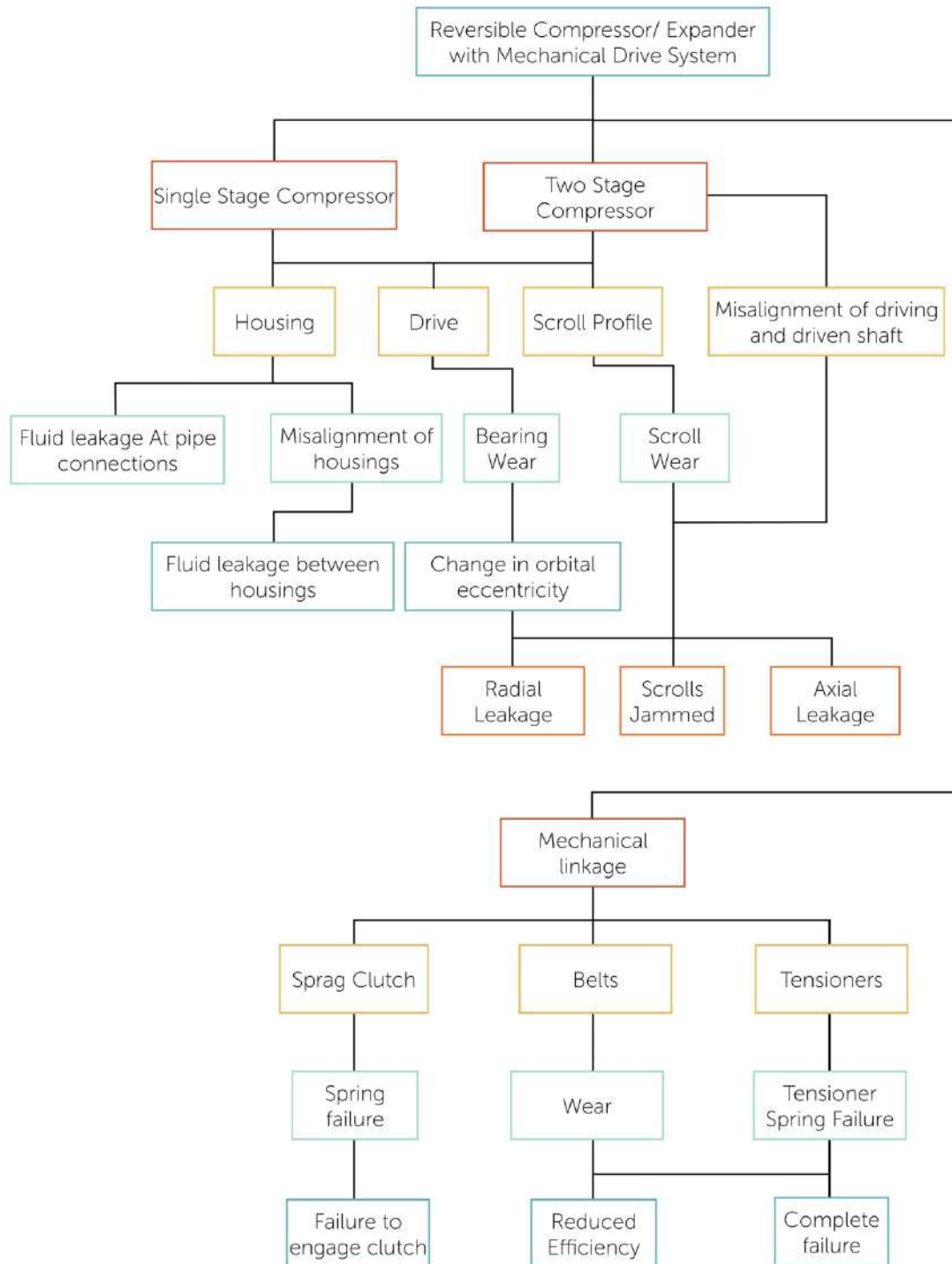


Figure 25: Failure Trouble Tree

Conclusion

This paper discussed the development of a model to optimise scroll profile design for the use in a pumped heat thermal energy storage system for use in rural Africa. From the model a scroll was successfully developed and used to design a full mechanical system comprising two reversible scroll compressor/ expanders and a motor generator with automatic gear variation between charge and discharge cycles. Though a full design was completed, future research is recommended before progressing with the design. Given greater access to resources, the scroll compressors could be analysed with CFD that would give greater insight into the functionality of the system, than that which has been presented here.

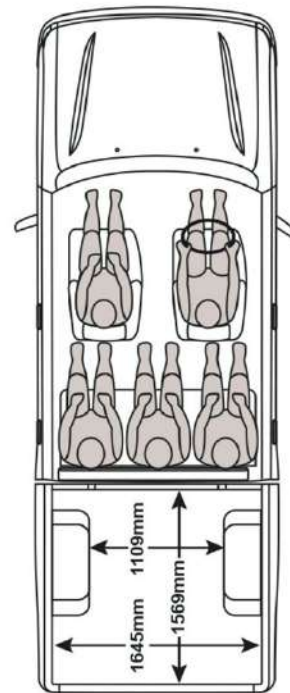
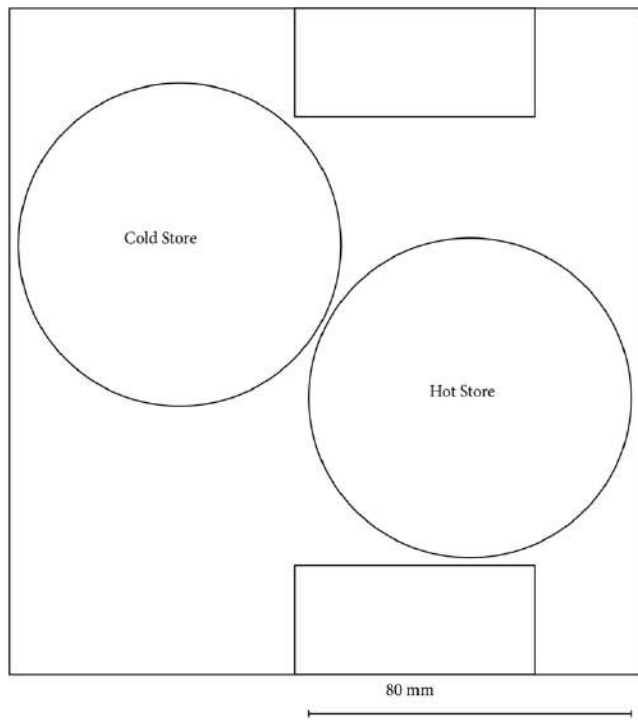
Bibliography

1. Rosie Knight, Project manager/ pressure vessel design report. (n.d.).
2. Donny Wong, *System Intergration Report*.
3. Jack Martin, Tank Optimisation Report. (n.d.).
4. J. De Saulles, *Refrigeration Report*.
5. Jerry Chung, *Heat Exchanger Report*.
6. A. White, G. Parks, & C. N. Markides, Thermodynamic analysis of pumped thermal electricity storage. *Applied Thermal Engineering*, **53** (2013) 291–298. <https://doi.org/10.1016/j.applthermaleng.2012.03.030>.
7. B. Blunier, G. Cirrincione, Y. Hervé, & A. Miraoui, A new analytical and dynamical model of a scroll compressor with experimental validation. *International Journal of Refrigeration*, **32** (2009) 874–891. <https://doi.org/10.1016/j.ijrefrig.2008.11.009>.
8. H. Ritchie & M. Roser, Access to Energy. *Our World in Data*, (2019).
9. Rosie Knight et al., eCOOL_G17_Business Proposal. (n.d.).
10. Rosie Knight et al., Pumped heat thermal energy storage: Terchnical feasibility Study for use in Rural african location. (n.d.).
11. E. Adkins, K. Opielstrup, & V. Modi, Rural household energy consumption in the millennium villages in Sub-Saharan Africa. *Energy for Sustainable Development*, **16** (2012) 249–259. <https://doi.org/10.1016/j.esd.2012.04.003>.
12. S. Szabó, K. Bódis, T. Huld, & M. Moner-Girona, Energy solutions in rural Africa: Mapping electrification costs of distributed solar and diesel generation versus grid extension. *Environmental Research Letters*, **6** (2011). <https://doi.org/10.1088/1748-9326/6/3/034002>.
13. • Average electricity prices in Africa by key country 2016 | Statista. (n.d.). <https://www.statista.com/statistics/503727/retail-electricity-prices-in-africa-by-select-country/> (accessed May 24, 2020).
14. M. Sanni & K. Neureiter, How innovation in off-grid refrigeration impacts lives in Kenya. (2019).
15. Data | The World Bank. (n.d.). <http://datatopics.worldbank.org/sdgdatalatlas/archive/2017/SDG-01-no-poverty.html> (accessed May 24, 2020).
16. PWC, Sub-Saharan Africa’s third-largest economy will stay on a fast growth path. Key drivers will be further rises in oil production, recently announced reform programmes and political stability. (2012).
17. Most Popular Cars in Africa | Innov8tiv. (n.d.). <https://innov8tiv.com/most-popular-cars-in-africa/amp/> (accessed May 24, 2020).
18. M. P. Blimpo & M. Cosgrove-Davies, *Electricity Access in Sub-Saharan Africa: Uptake, Reliability, and Complementary Factors for Economic Impact* (2019). <https://doi.org/10.1596/978-1-4648-1361-0>.
19. D. Rysankova, E. Portale, & G. Carletto, Sustainable Energy For All : Measuring Energy Access Introduction to the Multi-Tier Framework. *Introduction to the Multi-Tier Framework*, (2016) 29.
20. STAGE G ATE 3 : D ESIGN L EAD R EPORT – T ECHNICAL F EASIBILITY S AM R IDDELL -W EBSTER - 11641. (n.d.).
21. B. Blunier, G. Cirrincione, & A. Miraoui, Novel Geometrical Model of Scroll Compressors for the Analytical Description of the Chamber Volumes. *International Compressor Engineering Conference*, (2006) 1745.
22. Y. Chen, N. P. Halm, E. A. Groll, & J. E. Braun, Mathematical modeling of scroll compressors - Part I: Compression process modeling. *International Journal of*

- Refrigeration*, **25** (2002) 731–750. [https://doi.org/10.1016/S0140-7007\(01\)00071-8](https://doi.org/10.1016/S0140-7007(01)00071-8).
23. M. Wannassi, Geometrical Analysis of a Scroll Compressor and Fluid Mechanical Modeling Geometrical Analysis of a Scroll Compressor and Fluid Mechanical Modeling. (2016). <https://doi.org/10.1007/978-3-319-17527-0>.
 24. I. H. Bell, V. Lemort, E. A. Groll, J. E. Braun, G. B. King, & W. T. Horton, Liquid-flooded compression and expansion in scroll machines - Part I: Model development. *International Journal of Refrigeration*, **35** (2012) 1878–1889. <https://doi.org/10.1016/j.ijrefrig.2012.07.010>.
 25. I. Bell, V. Lemort, & J. Braun, Development of Liquid-Flooded Scroll Compressor and Expander Models. *International Compressor Engineering Conference*, (2008) Paper 1872.
 26. S. Emhardt, G. Tian, & J. Chew, A review of scroll expander geometries and their performance. *Applied Thermal Engineering*, **141** (2018) 1020–1034. <https://doi.org/10.1016/j.applthermaleng.2018.06.045>.
 27. T. Yanagisawa, Optimum operating pressure ratio for scroll compressor - Yanagisawa, T., et al. - Purdue (1990).pdf. (1990).
 28. N. Cho, Y. Youn, B. Lee, & M. Min, The Characteristics of Tangential Leakage in Scroll Compressors for Air-conditioners. *Engineering Conference*, (2000) 807–814.
 29. N. Ishii, Refrigerant leakage flow evaluation for scroll compressors. *International compressor engineering conference*, (1996).
 30. E. Oralli, M. A. Tarique, C. Zamfirescu, & I. Dincer, A study on scroll compressor conversion into expander for Rankine cycles. *International Journal of Low-Carbon Technologies*, **6** (2011) 200–206. <https://doi.org/10.1093/ijlct/ctr008>.
 31. W. He & J. Wang, Optimal selection of air expansion machine in Compressed Air Energy Storage: A review. *Renewable and Sustainable Energy Reviews*, **87** (2018) 77–95. <https://doi.org/10.1016/j.rser.2018.01.013>.
 32. G. Pahl, *Engineering Design: A Systematic Approach* (Springer, 2004). <https://doi.org/10.1017/CBO9781107415324.004>.
 33. Fenner, Friction belt drives. *Friction Belt Drives*, (2019).
 34. Keyway and Key Size Dimensions. (n.d.) 4.
 35. G. Kosmadakis, G. Mousmoulis, D. Manolagos, I. Anagnostopoulos, G. Papadakis, & D. Papantonis, Development of Open-Drive Scroll Expander for an Organic Rankine Cycle (ORC) Engine and First Test Results. *Energy Procedia*, **129** (2017) 371–378. <https://doi.org/10.1016/j.egypro.2017.09.236>.
 36. P. Bin, A. Legros, V. Lemort, X. Xiaozheng, & G. Haifeng, Recent Advances on the Oil-Free Scroll Compressor. *Recent Patents on Mechanical Engineering*, **9** (2015) 37–47. <https://doi.org/10.2174/2212797609666151109204948>.
 37. Brushless DC Motor vs. AC Motor vs. Brushed Motor. (n.d.). <https://www.orientalmotor.com/brushless-dc-motors-gear-motors/technology/AC-brushless-brushed-motors.html> (accessed May 25, 2020).

Appendix I

Toyota Hilux storage bay dimensions



Bansaaso, Ghana



Dertu, Kenya



Ikaram, Nigeria (N 07°36'43" E 005°51'58")



Mayange, Rwanda (S 02°14'30" E 030°08'00")



Mbola, Tanzania (S 05°03'24" E 032°32'56")



Mwandama, Malawi (S 15°31'25" E 035°10'54")



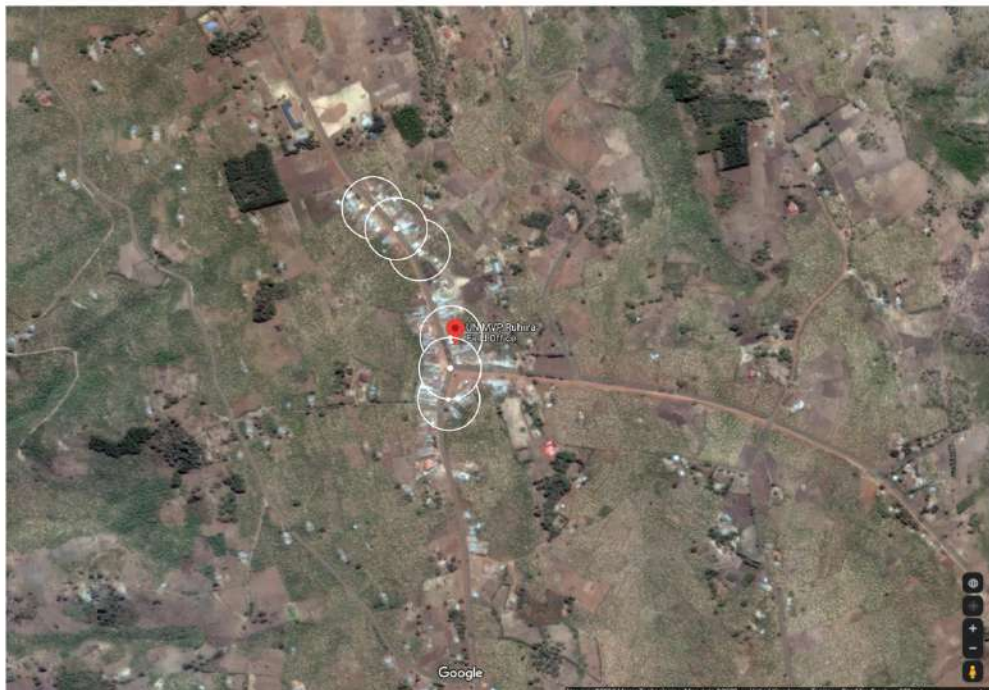
Pampaida, Nigeria (N 11°19'03" E 008°09'23")



Potou, Senegal (N 15°44'48" W 016°28'05")



Ruhiira, Uganda (S 00°52'54" E 030°39'26")



Tiby, Mali (N 13°35'14" W 005°46'30")



Appendix II

```
function [Rb, phi_i0, phi_e0, phi_is, phi_es, phi_max] =  
ScrollProfileGenertor(CompressionR)  
  
% [V_in, V_out] = InputVol(VDot_in, RPM,CompressionR); % Determines the  
input volume into the compressor per rotation  
  
InitalAngles = zeros(4,1);  
z = 1;  
Rb = 3;  
  
    [InitalAngles, Rb] = InvoluteFinder(Rb, InitalAngles); % Generates  
all phi_i0, phi_e0 combinations that are in contact  
  
    [StartingAngles] = StartingPointsFinder(InitalAngles, z); %  
Generates all phi_is and phi_es values that provide proper cut off  
  
    z =z ;  
end
```

```

% novel referance frame
function [InitalAngles, Rb, a] = InvoluteFinder(Rb, InitalAngles)

flag1 = 0;
phi_i0 = 0; %Sets inital conditions for first scroll
phi_e0 = 0;
theta = pi; % sets abitary value of theta for the moment
z = 1;
zz = 1;
%%%Loop Size

LoopSize = 720; % sets up inital arrays to reduce
xfe = zeros(1,LoopSize); % operstion time
yfe = zeros(1,LoopSize);
xfi = zeros(1,LoopSize);
yfi = zeros(1,LoopSize);
Sfe = zeros(2,LoopSize);
Sfi = zeros(2,LoopSize);
SfeMag = zeros(1,LoopSize);
SfiMag = zeros(1,LoopSize);
SfeGM = zeros(1,LoopSize);
SfiGM = zeros(1,LoopSize);
SmeGM = zeros(1,LoopSize);
SmiGM = zeros(1,LoopSize);
Gfe = zeros(1,LoopSize);
Gmi = zeros(1,LoopSize);
PfeCol = zeros(1,LoopSize);
PmiCol = zeros(1,LoopSize);
c = 1;

while phi_i0 <= 2*pi

    while phi_e0 <= 2*pi

        t = Rb*(abs(phi_i0) - abs(phi_e0));
        if t <= 4 && t >= 2

            Degrees = [1:1:720];
            phi = (Degrees/360)*2*pi; % radians

            R0 = abs(Rb*(phi_e0 - phi_i0 + pi)); % Orbital radius of the
rotating scroll
% radius ang=0:0.01:2*pi; % Generates and plots orbital
radius
%
% polarplot(R0,ang);

            %generates scrolls
            while c <= LoopSize

                xfe(1,c) = Rb *cos(phi(1,c)) + Rb*(phi(1,c) - phi_e0)*
sin(phi(1,c)) + 0.5 * R0 * -sin(theta); % generates external coordinates
                yfe(1,c) = Rb *sin(phi(1,c)) - Rb*(phi(1,c) - phi_e0)*
cos(phi(1,c)) + 0.5 * R0 * cos(theta);

```

```

        xfi(1,c) = Rb *cos(phi(1,c)) + Rb*(phi(1,c) - phi_i0)*
sin(phi(1,c)) + 0.5 * R0 * -sin(theta); % generates internal coordinates
        yfi(1,c) = Rb *sin(phi(1,c)) - Rb*(phi(1,c) - phi_i0)*
cos(phi(1,c)) + 0.5 * R0 * cos(theta);

        Sfe(1,c) = xfe(1,c); % stores in matrix
        Sfe(2,c) = yfe(1,c);

        Sfi(1,c) = xfi(1,c); % stores in matrix
        Sfi(2,c) = yfi(1,c);

        SfeMag(1,c) = (Sfe(1,c)^2 + Sfe(2,c)^2)^0.5; % magntiude of
polar coordinate
        SfiMag(1,c) = (Sfi(1,c)^2 + Sfi(2,c)^2)^0.5;

        if      Sfe(2,c) >= 0 && Sfe(1,c) >=0

                SfeGM(1,c) = atan(Sfe(2,c)/Sfe(1,c)); %Finda gamma
polar coordinate angle
                SfiGM(1,c) = atan(Sfe(2,c)/Sfe(1,c));

        elseif Sfe(2,c) >= 0 && Sfe(1,c) <=0

                SfeGM(1,c) = pi + atan(Sfe(2,c)/Sfe(1,c)); %Finda
gamma polar coordinate angle
                SfiGM(1,c) = pi + atan(Sfe(2,c)/Sfe(1,c));

        elseif Sfe(2,c) <= 0 && Sfe(1,c) <=0

                SfeGM(1,c) = pi + atan(Sfe(2,c)/Sfe(1,c)); %Find
polar coordinate angle
                SfiGM(1,c) = pi + atan(Sfe(2,c)/Sfe(1,c));

        elseif Sfe(2,c) <= 0 && Sfe(1,c) >=0

                SfeGM(1,c) = 2*pi + atan(Sfe(2,c)/Sfe(1,c)); %Find
polar coordinate angle
                SfiGM(1,c) = 2*pi + atan(Sfe(2,c)/Sfe(1,c));

        end

        SmeGM(1,c) = SfeGM(1,c) + pi; % finds angular polar
coordinate for rotating scrole
        SmiGM(1,c) = SfiGM(1,c) + pi;

        if SmeGM(1,c) >= 2*pi % enusres
rotating scroll remains between zero and 2pi
                SmeGM(1,c) = SmeGM(1,c) - 2*pi;
        end
        if SmiGM(1,c) >= 2*pi
                SmiGM(1,c) = SmiGM(1,c) - 2*pi;
        end

        c = c+1;

end

SmeMag = SfeMag; % finds magnitue for rotation
scrole
SmiMag = SfiMag;
Smi = - Sfi;

```

```

Sme = -Sfe;

%%Polar coordinates

Pfe(1,:) = SfeMag(1,:);
Pfe(2,:) = SfeGM(1,:);
Pfi(1,:) = SfiMag(1,:);
Pfi(2,:) = SfiGM(1,:);
Pme(1,:) = SmeMag(1,:);
Pme(2,:) = SmeGM(1,:);
Pmi(1,:) = SmiMag(1,:);
Pmi(2,:) = SmiGM(1,:);

n = 1;
m = 1;
p = 1;

while n <= LoopSize
    while m <= LoopSize

        if Pmi(1,n) <= Pfe(1,m) + 0.1 && Pmi(1,n) >=
Pfe(1,m) - 0.1 && Pmi(2,n) <= Pfe(2,m) + 0.1 && Pmi(2,n) >= Pfe(2,m) - 0.1
            PfeCol(1,p) = m + 1;
            PmiCol(1,p) = n;

            % find gradient of all points on lines
            if PmiCol(1,p) >= 2

                % prevents error with gradient calculation
                Gfe(1,p) = (Sfe(2,PfeCol(1,p)) -
Sfe(2,PfeCol(1,p)-1))/(Sfe(1,PfeCol(1,p)) -Sfe(1,PfeCol(1,p)-1));

                Gmi(1,p) = (Smi(2,PmiCol(1,p)) -
Smi(2,PmiCol(1,p)-1))/(Smi(1,PmiCol(1,p)) -Smi(1,PmiCol(1,p)-1));

                if Gmi(1,p) <= Gfe(1,p) + 0.01 && Gmi(1,p)
>= Gfe(1,p) - 0.01

                    InitalAngles(1,z) = Rb;
                    InitalAngles(2,z) = phi_i0;
                    InitalAngles(3,z) = phi_e0;
                    InitalAngles(4,z) = R0;

                    z = z + 1;
                    flag1 = 1;
                    break
                end
            end
            p = p + 1 ;
        end
        m = m + 1;
    end
    if flag1 == 1
        flag1 = 0;
        break
    end
    m = 1;
    n = n + 1;
end

```

```

                end
            end
            phi_e0 = phi_e0 + 0.1*pi;
        end

        phi_e0 = 0;
        phi_i0 = phi_i0 + 0.1*pi;
        disp(phi_i0)
    end

%
% polarplot(Pfe(2,60:720),Pfe(1,60:720),'r')
% hold on
% polarplot(Pfi(2,60:720),Pfi(1,60:720),'r')
% polarplot(Pme(2,60:720),Pme(1,60:720),'b')
% polarplot(Pmi(2,60:720),Pmi(1,60:720),'b')
% % % polarplot(ContactPoint(2,:),ContactPoint(1,),'x')
% % % polarplot(IA1(2,:),IA1(1,));
% % % polarplot(IA2(2,:),IA2(1,));

end

```

```

% starting angles
function [StartingAngles] = StartingPointsFinder(InitalAngles, z)

StartingAngles = zeros(5,1);
[j,LoopNum] = size(InitalAngles);
RowNum = LoopNum*720+j;          % Determines number of possible
combinations of inital angles

q = 1;
a = 1;
while q <= LoopNum

    %Inital angles
    Rb      = InitalAngles(1,q);
    phi_i0  = InitalAngles(2,q);
    phi_e0  = InitalAngles(3,q);
    R0      = InitalAngles(4,q);
    phi_is  = 0.01;
    phi_es  = 0;
    InitalAngles(5,q) = phi_is;
    InitalAngles(6,q) = phi_es;
    m = 1;

    while phi_is <= 2* pi
        while phi_es <= 2* pi

            % Circle generating parameters
            e_1 = phi_es - phi_e0;
            e_2 = phi_is - phi_i0;
            e_3 = phi_is - phi_es;

            % radius of circle Cc
            Rc = abs((Rb*(2+ e_2^2+ e_1^2- 2*(1+ e_1*
e_2)*cos(e_3)- 2*(e_2- e_1)*sin(e_3)))/(2*(e_2-e_1*cos(e_3)-sin(e_3))));
            Cc_0x = Rb* cos(phi_is) + (Rc - Rb* (phi_is -phi_i0))*
-sin(phi_is); % cartesian origin of Circle Cc
            Cc_0y = Rb* sin(phi_is) + (Rc - Rb* (phi_is -phi_i0))*
cos(phi_is);

            if      Cc_0y >= 0 && Cc_0x >=0

                Oc_Theta = atan(Cc_0y /Cc_0x); %Finda polar
coordinate origin point if in first quadrant

            elseif Cc_0y >= 0 && Cc_0x <=0

                Oc_Theta = atan(Cc_0y /Cc_0x) + pi; %Finda
polar coordinate origin point if in second quadrant

            elseif Cc_0y <= 0 && Cc_0x <=0

                Oc_Theta = atan(Cc_0y /Cc_0x) + pi; %Finda
polar coordinate origin point if in third quadrant

            elseif Cc_0y <= 0 && Cc_0x >=0

                Oc_Theta = atan(Cc_0y /Cc_0x) + 2*pi; %Finda
polar coordinate origin point if in forth quadrant

        end
    end
end

```

```

Cc circle
    Cc(1,1) = Rc;           % stores polar co ordinats of
    Cc(2,1) = Oc_Theta;    %Polar coordiante angle
    Cc(3,1) = Cc_0x;       % Cartesian origin coordinates
    Cc(4,1) = Cc_0y;

    ang=0:0.01:2*pi; %Generates and plots Circel Cc radius
    Cc_pointX = Cc(1,1)*cos(ang) + Cc(3,1); %Cartesian
coordnaites for Cc
    Cc_pointY = Cc(1,1)*sin(ang) + Cc(4,1);

    g = 1;

    while g <= 629
        Cc(6,g) = (Cc_pointX(1,g)^2 +
Cc_pointY(1,g)^2)^0.5; % magntiude of polar coordinate

        if Cc_pointY(1,g) >= 0 && Cc_pointX(1,g)
>=0
            Cc(5,g) =
atan(Cc_pointY(1,g)/Cc_pointX(1,g)); %Finda gamma polar coordinate angle
        elseif Cc_pointY(1,g) >= 0 && Cc_pointX(1,g)
<=0
            Cc(5,g) = pi +
atan(Cc_pointY(1,g)/Cc_pointX(1,g)); %Finda gamma polar coordinate angle
        elseif Cc_pointY(1,g) <= 0 && Cc_pointX(1,g)
<=0
            Cc(5,g) = pi +
atan(Cc_pointY(1,g)/Cc_pointX(1,g)); %Finda gamma polar coordinate angle
        elseif Cc_pointY(1,g) <= 0 && Cc_pointX(1,g)
>=0
            Cc(5,g) = 2*pi +
atan(Cc_pointY(1,g)/Cc_pointX(1,g)); %Finda gamma polar coordinate angle
        end
        g = g + 1;
    end % Generates polar angle coordinate

    % Find points where Cc and involutes intersect
    [StartingAngles, z, phi_is, phi_es] =
StartingAngleIntersectionPoint(Rb, phi_i0, phi_e0, phi_is, phi_es, R0, Cc,
StartingAngles, z, Cc_pointX, Cc_pointY);

%
    [inner volume] =

    phi_es = phi_es + 0.1*pi;

    a = a + 1;

end

```

```
        phi_es = 0;
        phi_is = phi_is + 0.1*pi;
%        disp(phi_is)

    end
    q = q + 1;
    disp(q)

end

end
```

Appendix III

$$\text{Max Power} = 4 \text{ kW}$$

$$\text{Low end RPM} = 130$$

$$T = \frac{P \times 60}{2\pi \times \text{RPM}}$$

$$= \frac{4000 \times 60}{2\pi \times 130}$$

$$= 293.82 \text{ Nm}$$

f_T , Torque factor 1.5

$$\begin{aligned} T_{\text{operational}} &= 440.7 \text{ Nm} \\ &= 440700 \text{ Nmm (Mpa)} \end{aligned}$$

$$\text{EMT } T = 500 \text{ Mpa}$$

$$D_{\text{GT}}^3 = \frac{T \times 16}{\pi \tau \times 800}$$

$$= \frac{440700 \times 16}{500 \pi}$$

$$D = 16.5$$

Safety factor, $f_s = 1.5$

$$\therefore D = 25 \text{ mm}$$